

ALERT Open Dataset and Input-Size-Agnostic Vision Transformer for Driver Activity Recognition using IR-UWB

Jeongjun Park^{*§}, Sunwook Hwang^{*§}, Hyeonho Noh^{†§}, Jin Mo Yang[‡], Hyun Jong Yang[‡], Saewoong Bahk^{‡¶}

^{*} System LSI, Samsung Electronics, South Korea

[†] Department of ICE, Hanbat National University, Daejeon, Republic of Korea

[‡] Department of ECE and INMC, Seoul National University, Seoul, Republic of Korea

[§] This work was done when the author was with Department of ECE and INMC, Seoul National University

[¶] Senior Member, IEEE

Abstract—Distracted driving contributes to fatal crashes worldwide. To address this, researchers are using driver activity recognition (DAR) with impulse radio ultra-wideband (IR-UWB) radar, which offers advantages such as interference resistance, low power consumption, and privacy preservation. However, two challenges limit its adoption: the lack of large-scale real-world UWB datasets covering diverse distracted driving behaviors, and the difficulty of adapting fixed-input Vision Transformers (ViTs) to UWB radar data with non-standard dimensions.

This work addresses both challenges. We present the *ALERT* dataset, which contains 10,220 radar samples of seven distracted driving activities collected in real driving conditions. We also propose the input-size-agnostic Vision Transformer (*ISA-ViT*), a framework designed for radar-based DAR. The proposed method resizes UWB data to meet ViT input requirements while preserving radar-specific information such as Doppler shifts and phase characteristics. By adjusting patch configurations and leveraging pre-trained positional embedding vectors (PEVs), *ISA-ViT* overcomes the limitations of naive resizing approaches. In addition, a domain fusion strategy combines range- and frequency-domain features to further improve classification performance.

Comprehensive experiments demonstrate that *ISA-ViT* achieves a 22.68% accuracy improvement over an existing ViT-based approach for UWB-based DAR. By publicly releasing the *ALERT* dataset and detailing our input-size-agnostic strategy, this work facilitates the development of more robust and scalable distracted driving detection systems for real-world deployment.

Index Terms—Open dataset, IR-UWB radar, driver activity recognition (DAR), benchmarking

I. INTRODUCTION

According to the World Health Organization (WHO), 1.19 million people die every year due to vehicle accidents [1]. Additionally, the National Highway Traffic Safety Administration (NHTSA) [2] in the United States estimates that approximately 6 million traffic accidents are reported to police each year, resulting in 38,000 to 40,000 fatalities annually. Among these vehicle accidents, distracted driving accounts for about 10% of fatal incidents, often involving some form of driver distraction. Given its unavoidable nature, detecting and mitigating distracted driving is a crucial task.

To prevent driver distraction, many researchers have studied Driver Activity Recognition (DAR) using various approaches:

camera vision [3], [4], acoustic signals [5], [6], and Radio Frequency (RF) signals [7], [8], [9], [10], [11], [12], [13]. However, these approaches have several limitations. To prevent driver distraction, many researchers have studied Driver Activity Recognition (DAR) using various approaches: camera vision [3], [4], acoustic signals [5], [6], and Radio Frequency (RF) signals [7], [8], [9], [10], [11], [12], [13]. However, these approaches have several limitations. Camera vision struggles with poor lighting and raises privacy concerns regarding the potential restoration in intelligent vehicle systems [14], [15]. Acoustic signal-based methods can be disrupted by ambient noise and also pose privacy risks due to continuous microphone activation. RF signal-based approaches have predominantly been studied using WiFi. However, utilizing WiFi, primarily operating within the busy 2.4 GHz industrial, scientific, and medical (ISM) band, within a vehicle can potentially cause interference with other vehicle devices using Bluetooth or similar busy ISM band communications.

In this paper, we exploit the Impulse Radio Ultra-Wideband (IR-UWB) radar for DAR while driving to tackle these problems. UWB offers several advantages: i) robustness against interference and multipath fading due to its wide bandwidth (≥ 500 MHz), ii) operation within the 6.5–9 GHz range with low transmit power (-41.3 dBm/MHz), ensuring coexistence with popular wireless formats such as satellite navigation, WiFi, Bluetooth, and ZigBee [16]. iii) inherent privacy protection, as it avoids capturing visual or audio data. Consequently, UWB-based Human Activity Recognition (HAR) has garnered significant attention [17], [18], [19], [11], [12], [20], [21], [22], [23], [24], [25], [26].

Challenges. Despite the potential of UWB, applying UWB to DAR presents two key challenges. The first is the lack of comprehensive research addressing diverse and complex distracted driving activities using UWB sensing data in real-world driving environments. Collecting such datasets demands substantial time and effort, with the workload increasing proportionally to the number of labels and environmental complexity. This difficulty may partly explain why many studies [5], [6], [20], [12] have focused solely on single distracted driving activities. However, given the varied nature of distracted driving behaviors, monitoring only one type of behavior is insufficient to prevent traffic accidents.

Corresponding authors: Sunwook Hwang (sunwookh@snu.ac.kr) and Saewoong Bahk (sbahk@snu.ac.kr).

Although existing DAR dataset [11] have collected dataset on various distracted driving activities, the dataset is gathered in simulated environments. Such an approach fails to account for critical real-world factors, such as road conditions, vehicle vibrations, and other environmental influences. This limitation raises concerns about the generalizability and reliability of these datasets for real driving scenarios.

The second challenge lies in the incompatibility of UWB data with state-of-the-art models for DAR. Recently, Vision Transformers (ViTs) [27], [28], [29], [30] have emerged as state-of-the-art models across multiple vision task benchmarks, gaining significant attention for their performance in classification tasks. Consequently, many researchers have attempted to transfer the powerful capabilities of ViTs to other domains, including UWB domain. However, resizing UWB radar images to align with standard ViT input dimensions is non-trivial, as naive interpolation can distort essential radar-specific information such as Doppler shifts, phase, and signal attenuation. Pre-trained ViTs rely on positional embedding vectors (PEVs) optimized for fixed-size natural images, and mismatches in spatial relationships degrade performance.

Nevertheless, many studies [31], [32], [33], [34], [35] using ViTs for UWB sensing have treated this resizing step as a minor implementation detail, not detailing any domain-specific approach to handle the unique geometry of UWB data. This oversight can result in significant performance loss, highlighting the need for an input-size-agnostic approach that preserves crucial radar-domain features while seamlessly integrating with pre-trained ViTs.

Approaches. To address the first challenge, the lack of real-driving datasets, we collect the *ALERT* dataset, comprising 10,220 samples of 7 distracted driving activities captured in real-driving environments. We present benchmarking performance of widely used 8 learning algorithms—CNN-based [36], [37], [38], [39], RNN-based [24], [22], [23], and transformer-based approaches [40], [27]—that are applicable in UWB DAR. Additionally, we design experiments to provide the effective utilization of the *ALERT* dataset across these 8 algorithms such as analyzing observation time, multipath effects, and frequency area. Consequently, we make the *ALERT* dataset publicly available to promote its adoption and foster further advancements in UWB DAR research.

To overcome these compatibility issues, we propose the Input-Size-Agnostic Vision Transformer (*ISA-ViT*), which introduces a customized resizing scheme for UWB data, preserving domain-specific features such as range and frequency information. By strategically adjusting patch dimensions and leveraging the pre-trained PEVs, *ISA-ViT* maintains spatial coherence and avoids the signal corruption often caused by naive resizing. This design also modifies the linear projection layers to accommodate altered patch sizes, ensuring seamless integration with pre-trained ViT weights. Our experiments reveal that this tailored approach significantly improves performance while retaining straightforward implementation.

Furthermore, we develop a domain fusion strategy that leverages both range and frequency domain representations, which preserve distinct yet complementary signal characteristics. By applying our input-size-agnostic resizing and then fusing the

extracted features, we capitalize on the synergy between the two domains, boosting classification accuracy and reinforcing the benefits of an appropriately resized radar input.

The contributions of this work are summarized as follows:

- We present the *ALERT* dataset, the first UWB dataset capturing comprehensive driving activities in real-driving environments. With 10,220 samples across 7 activities, we evaluate its performance using 8 learning algorithms, spanning CNN-based, RNN-based, and transformer-based methods. By making the dataset publicly available, we aim to promote its adoption and support diverse experimentation tailored to various research needs.
- We propose *ISA-ViT*, a novel model addressing challenges in adapting pre-trained ViTs to UWB data with varying input sizes. *ISA-ViT* introduces a resizing method that avoids information loss and incorporates a domain fusion technique combining range and frequency domain features, significantly enhancing classification accuracy.
- Through extensive experiments, we demonstrate *ISA-ViT*'s superior performance, achieving a classification accuracy of 76.28% and distracted driving detection accuracy of 97.35%. Additionally, we present various benchmarking results and trade-offs for selecting suitable models in UWB DAR. Our work provides insights for future studies through benchmarking and the provision of the open *ALERT* dataset.

II. RELATED WORKS

DAR using UWB radar. Recently, several DAR systems utilizing UWB technology have emerged [12], [11], [20], [41]. Xu *et al.* [20] present UHead, a driver attention monitoring system based on UWB radar. Unlike traditional methods that rely on specialized sensors or cameras, UHead tracks the driver's head motion to infer attention. It extracts time-frequency data from UWB radar signals to estimate the direction and angle of head rotations. However, detecting a driver's distracted behavior solely based on head rotation has its limitations. Drivers can exhibit distracted behaviors without rotating their heads significantly such as using a mobile phone or smoking while driving.

Similarly, Hu *et al.* [12] design a system for fine-grained eye-blink monitoring in driving scenarios using customized IR-UWB radar. The system extracts eye-blink signals while filtering out interference from body movements and environmental factors. However, this approach is limited as it only targets drowsiness, overlooking other potential distractions that may occur during driving.

Khan *et al.* [41] present a radar-based system for robust heart rate detection intended for in-car monitoring. They propose a novel time-series-based algorithm instead of traditional frequency-domain methods, using a deep learning classifier to detect heart rate patterns. Additionally, they optimize the radar sensor's location inside the car to reduce interference from random body motions.

However, the above studies have focused solely on a single distracted driving activity. Given the diverse causes of traffic accidents resulting from distracted driving, targeting only one type of activity is insufficient to effectively prevent serious

traffic incidents. To address this issue, there is a need for studies that encompass a comprehensive range of distracted driving activities.

The study in [11] introduces an IR-UWB radar-based monitoring system capable of detecting a wide range of in-car activities. It also provides an open dataset for DAR in a simulated driving environment, covering 6 distracted driving activities: driving, autopilot, sleeping, driving while using a smartphone, smartphone use, and talking to a passenger. To the best of our knowledge, this is the first open dataset for UWB DAR in a simulated driving environment addressing six distracted driving activities.

However, simulated-driving environments fail to accurately represent real-world driving conditions, which involve factors such as ground vibrations, vehicle vibrations, and driving realism. For example, Morales-Alvarez *et al.* [42] report that the recognition accuracy of driver observation models decreased from 85.7% to 46.6% when transferred from simulation to real-world scenarios. Similarly, Stocco *et al.* [43] emphasize the “reality gap” in simulation-based testing for autonomous systems, noting that critical cues like vibration, cabin constraints, and natural driver reactions are often missing in simulated settings.

Additionally, imposing specific restrictions on driver activities (e.g., requiring the use of the right hand while talking or mandating two-handed smartphone use) may make the dataset more distinguishable but less realistic. Consequently, a realistic *de facto* standard open dataset is essential to advance UWB DAR studies. To address this need, we introduce the *ALERT* dataset in the following section, designed with realistic properties in mind.

Compared to the dataset from [11], the *ALERT* dataset focuses on more detailed distracted driving activities in *real-world driving environments*. It includes data for 7 activities: relaxation (autopilot), driving, nodding, smoking, drinking, panel control, and smartphone use. Additionally, the *ALERT* dataset provides both range and frequency domain data, enabling a variety of experimental approaches to be explored using the data.

The use of ViT with UWB. Various works [31], [32], [33], [34], [35] introduce the use of ViT with UWB. Li *et al.* [31] introduce MobileViTX, an improved version of the MobileViT architecture, specifically designed for human activity recognition (HAR) using IR-UWB radar. The Zhao *et al.* [32] explore the feasibility of classifying human activities using data captured by a distributed UWB radar system. They compare ViT with CNN-based architectures and validate the robustness of these models, demonstrating ViT’s ability to generalize to unseen participants.

Moreover, Lai *et al.* [33] focus on developing a non-invasive sleep posture recognition system using multiple UWB radars. They employ machine learning models for classification, including CNN-based networks and ViT. Kim *et al.* [35] introduce a new approach for 3D human pose estimation using IR-UWB radar, leveraging a transformer-based deep learning model.

The above studies have attempted to apply UWB data to ViT. However, none of them provide sufficient discussion on how to

TABLE I
UWB RADAR PARAMETERS FOR DATA COLLECTION

Parameters	Values
Tx center frequency	8.748 GHz
Tx bandwidth (−10 dBm)	1.5 GHz
Energy per pulse	0.3–1.7 pJ
Frame per second	100 Hz
Range (bins)	0–9 m (178)
Sampling frequency	23.328 GHz
Pulse repetition frequency	15.1875 MHz

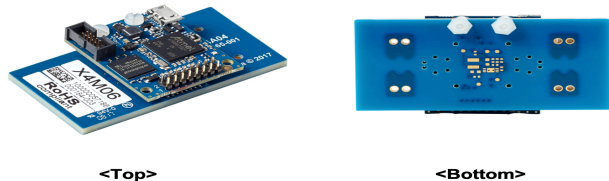


TABLE II
XETHRU X4M06 UWB RADAR SENSOR BY NOVELDA.

adapt UWB data, which has a different input size from images, for use in ViT. The unique study [44] addresses how to apply audio data to ViT when the input shapes differ. Gong *et al.* [44] introduce the audio spectrogram transformer (AST) model, the first purely attention-based model for audio classification. They cut and interpolate the PEVs for height or width in the AST model. By doing so, they transfer 2D spatial knowledge from the pre-trained ViT to the AST model, even when the input shapes are different. However, excessive cutting or interpolation of PEVs may incur the ruin of spatial information in pre-trained ViT [30]. Therefore, we need to explore a method that is not affected by input size while still utilizing the pre-trained parameters of the ViT.

III. ALERT OPEN DATASET

To collect comprehensive activities related to distracted driving in real-driving environments, we introduce the *ALERT* dataset in this section.

A. Sensor Specification

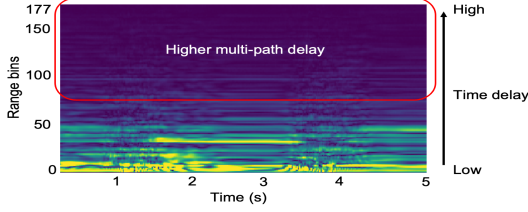
We capture the *ALERT* dataset using the UWB radar sensor Xethru X4M06, developed by Novelda [45], as depicted in Fig. II. The X4 series are the off-the-shelf devices in UWB radar technology and are widely utilized in several UWB HAR studies [11], [17], [19]. The radar features two directional patch antennas (Tx and Rx), optimized for frequencies between 7.25–10.2 GHz with an opening angle of 65° in both azimuth and elevation. The detailed parameters of the radar are presented in Table I.

B. Dataset Manipulation

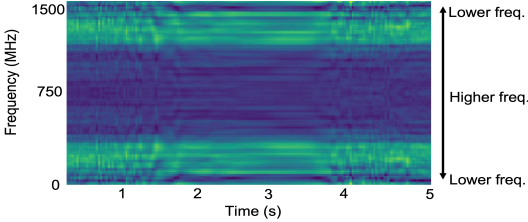
We need to process the UWB data from radar sensors to extract and provide various types of information. The IR-UWB radar periodically transmits the impulse signal; sth pulse has the slow-time index s . When the radar transmits the sth pulse, it comes back to radar as several signals due to multi-path. We can generalize the multi-path signal as f th multi-path; f th multi-path has the fast-time index f . To sum up, the fast-time

	$1, f$	$2, f$	$3, f$...	$s-1, f$	s, f
	$1, f-1$	$2, f-1$	$3, f-1$...	$s-1, f-1$	$s, f-1$
	\vdots	\vdots	\vdots	\ddots	\vdots	\vdots
	$1, 3$	$2, 3$	$3, 3$...	$s-1, 3$	$s, 3$
	$1, 2$	$2, 2$	$3, 2$...	$s-1, 2$	$s, 2$
	$1, 1$	$2, 1$	$3, 1$...	$s-1, 1$	$s, 1$
Fast-time (f th multi-path)						
	Slow-time (s th pulse)					

Fig. 1. Manipulation of UWB signal with two-dimensional fast-time vs. slow-time.



(a) Range data



(b) Frequency data

Fig. 2. Range and frequency data from UWB signal.

index indicates f th multi-path signal, and the slow-time index indicates s th transmitted impulse signal as shown in Fig. 1. Simply, we can express the received signal as follows

$$r_s(t) = \sum_{f=1}^F \alpha_f \delta(t - \tau_f) * m_s(t) + n_s(t), \quad (1)$$

where $r_s(t)$ is a received signal from s th impulse, F is the number of multi-path for transmitting signal $m_s(t)$, $n_s(t)$ is noise, and α_f is the attenuation factor of f th multi-path. For each pulse, the multi-path indicates time delay so that we call the fast-time vs. slow-time 2D data as range data. Moreover, we can also obtain the frequency data by performing fast Fourier transform (FFT) to range data. As frequency data can express the Doppler frequency shift, we can get the movement characteristic of object.

We obtain the range data as shown in Fig. 2(a). The Y-axis of Fig. 2(a) represents the fast-time index, which indicates range bin from the radar device. Although the distance between the radar and the driver is at most less than 2 meters, the upper part of Fig. 2(a) may provide critical information for detecting activities according to the learning algorithm (e.g., the size of convolutional layer filters). To this end, we provide our dataset, which allows users to customize the information about the range according to their specific needs. We provide the whole range bins of 178 by default (about 9 m).



(a) Detailed in-vehicle environment and radar deployment



(b) Urban route



(c) Campus

Fig. 3. Driving environment and driving course for data collection.

For frequency data, discrete FFT transforms the signal into periodic expressions, as illustrated in Fig. 2(b). Movements can be expressed across a range of frequencies, so significant information can be obtained from specific frequency bands relevant to the activity. To this end, we provide a dataset that enables users to freely crop the frequency information to facilitate versatile data utilization; we provide 178 frequency bins by default. Additionally, we offer an adjustable observation time (slow-time window), allowing users to select data with an observation time that best suits their needs.

C. Data Collection

Our dataset exhibits a significant strength: We collect the dataset in a real-driving environment. Accordingly, we mount the radar within an actual vehicle, as depicted in Fig. 3(a). We strategically attach the radar to the vehicle's air vent. This position does not obstruct the driver's view while driving and is well-situated to capture the driver's upper body and movements. Moreover, considering that modern smartphones are already equipped with built-in UWB chipsets, we have explored the potential integration of UWB radar into mobile phones. Since most drivers already use smartphone holders clipped to the air vent, mounting the UWB radar in the same location is not only practical but also aligns well with real-world usage patterns, supporting easy installation and potential commercialization.

We have driven along the designated red line and collected the dataset, as shown in Figs. 3(b) and 3(c). The urban

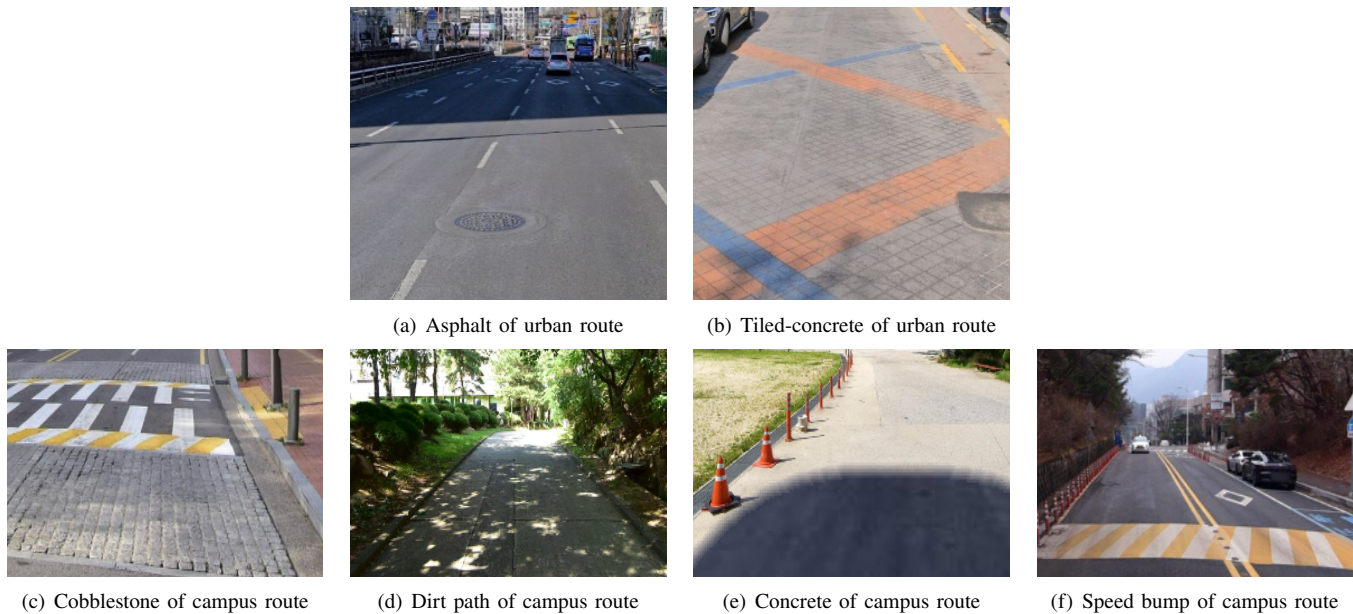


Fig. 4. Various road conditions of urban and campus routes.

route spans 12 km and provides relatively smooth driving conditions, similar to highway driving, due to light traffic and few traffic signals. The route is predominantly flat, with a single uphill and downhill section, both having an approximate gradient of 10 degrees. Most of the road surface is paved with asphalt, although some areas are made of tiled-concrete as shown in Fig. 4(a) and 4(b). As a result, vehicle vibrations remain generally stable and are primarily influenced by the irregularities of the road surface.

The campus route forms a 6 km loop with a speed limit of 30 km/h, enabling low-speed driving. Due to the presence of frequent pedestrian crossings, vehicles often experience stop-and-go movement, creating conditions similar to traffic congestion. The route is composed of approximately 50% sloped sections—both inclines and declines—and 50% flat terrain. The average gradient of the uphill segments is around 10.2 degrees, while the downhill sections average about 9.2 degrees. Although the majority of the road surface is asphalt, the route also includes cobblestone areas, dirt roads, and numerous speed bumps as shown in Fig. 4(c)–4(f), leading to diverse and irregular vibrations originating from the road surface.

To ensure a safer experiment, we adhere to the speed limit and have attached a sign to the vehicle indicating that an experiment is underway while driving.

To detect the driver’s activity while driving, we select seven labels: Relaxation (*Relax*), steering wheel control (*Drive*), nodding (*Nod*), smoking (*Smoke*), drinking (*Drink*), panel control (*Panel*), and using smartphone (*Phone*). Except for *Drive*, the drivers must not perform all other activities while driving. According to the National Highway Traffic Safety Administration (NHTSA) [2], the Governors Highway Safety Association (GHSA) [46], the Centers for Disease Control and Prevention (CDC) [47], and the Insurance Institute for Highway Safety (IIHS) [48], National Institutes of Health

(NIH) [49] in the United States and World Health Organization (WHO) [50], five of these activities—*Nod*, *Smoke*, *Drink*, *Panel*, and *Phone*—are considered distracted driving and cause severe traffic accidents commonly observed in daily life.

Additionally, we include the *Relax* label to address the current issue of *blind trust* in autonomous driving technology. Many drivers using autonomous driving technology tend to disengage from driving and take their hands off the steering wheel. This behavior poses significant risks, highlighting the need for monitoring even seemingly benign activities like relaxation while driving. We explain seven activities in detail as follows.

- *Relax* refers to a posture where drivers remove their hands from the steering wheel to rest, relying on autonomous driving technology. The drivers take breaks in various ways, such as freely taking their hands off the steering wheel and folding their arms, humming along to music, or talking on the phone using hands-free devices.
- *Drive* involves drivers placing both hands on the steering wheel and driving through the courses shown in Fig. 3. The drivers are free to make left turns, right turns, or U-turns along the course according to their driving habits.
- *Nod* is a key indicator of drowsy driving. The drivers nod their heads while keeping their hands on the steering wheel.
- *Smoke* denotes smoking activities. The drivers freely smoke regular cigarettes and electronic cigarettes according to individual smoking habits. This activity involves inhaling and exhaling smoke, as well as putting ashes into the ashtray located in front of the armrest.
- *Drink* involves drinking activities, either directly from a bottle or using a straw. The drivers place the bottle or cup in the cup holder, drink water or other beverages, and then return it to the cup holder located in front of the armrest.
- *Panel* encompasses various tasks such as adjusting the stereo volume, air conditioning, controlling the navigation, and

TABLE III
SAMPLE DISTRIBUTION FOR VOLUNTEERS AND ACTIVITIES.

Volunteers	P1	P2	P3	P4	P5	P6	P7	P8	P9
# of samples	1,400	1,400	1,200	1,140	680	740	1,160	1,280	1,220
Activities	Relax	Drive	Nod	Smoke	Drink	Panel	Phone		
# of samples	1,800	1,400	1,020	1,800	1,400	1,400	1,400	1,400	
Total samples	10,220								

pressing panel buttons.

- *Phone* involves various smartphone activities. The drivers exchange messages, swipe display to search for music playlist, surfs web, etc.

The activities of *Drive*, *Smoke*, *Phone*, and *Panel* are continuous and can be sustained over a long period. For these activities, we have collected data continuously during actual driving. In contrast, *Drink* and *Nod* are inherently short in duration. For these activities, we asked participants to perform the actions 2–3 times within a 10-second window in a natural and realistic manner. For *Nod*, the data captured moments when the driver’s steering control weakened, their head dropped, and then returned to the original position. For *Drink*, the sequence included retrieving a drink from the cup holder, taking a sip, and placing it back.

Additionally, *Relax*, and *Nod* are impractical to perform safely during real driving. Therefore, data for *Relax* and *Nod* are collected while the engine is running but the vehicle is stationary. In summary, for short-duration activities like *Drink* and *Nod*, participants are only given a time window and acted based on their natural behavior without detailed instructions.

Importantly, we provide minimal guidance on using the right hand for *Smoke*, *Drink*, and *Panel* activities, as the ashtray, cup holder, and panel are typically located on the driver’s right-hand side as shown in Fig. 3(a). For this reason, drivers do not intentionally cross their arms with their left hand to perform these actions. Other than these instances, the drivers can perform the actions freely, reflecting habitual behaviors in the aforementioned activities.

We have obtained the dataset from nine volunteers, yielding a total of 10,220 samples (per 5 seconds) as shown in Table III. The participants consist of individuals with heights ranging from 165 to 188 cm and weights between 53 and 100 kg. Their ages range from 26 to 35 years old, with an average age of 32. Their driving experience spans from 1 to 10 years, with an average of 6 years. All participants are familiar with typical passenger vehicles, primarily sedans and SUVs. In addition, all participants reported prior experience with the types of distracted driving activities included in the ALERT dataset.

D. Dataset Representation

Through dataset manipulation, we obtain range and frequency data for each activity. We exemplify the representations with prominent features of 7 activities in Fig. 5. Each representation exhibits distinct patterns or shapes unique to each activity, which are difficult to differentiate with the human eye alone, thus necessitating the use of learning methods for distinction. Someone may consider a vision-task approach appropriate due to the 2D nature of the manipulated data. Conversely, others might view the dataset as suitable for

TABLE IV
DATASET COMPARISON OF *ALERT* AND RaDA

Features	ALERT	RaDA [11]
# of activities	7	6
# of subjects	9	10
Activity restrictions	Lenient	Moderate
# of samples	10,220 (5 s per sample)	10,406 (1 s per sample)
Dataset	Range-time & freq.-time	Range-Doppler
Driving environment	Real driving	Simulated driving
Sensor position	Air vent	Front of driver (visual obstruction)

sequential prediction due to its time-series information. Thus, we describe the various approaches in Section IV and evaluate the most appropriate method for UWB data in Section VI.

E. Dataset Comparison

In UWB DAR, the existence of standard open dataset is significant to accelerate the studies. In [11], they provide the first open dataset, RaDA, for UWB DAR including comprehensive 6 activities such as driving, autopilot, sleeping, driving & smartphone utilization, smartphone utilization, and talking to a passenger. However, it is not enough to serve as *de facto* standard open dataset compared to our dataset, *ALERT*. The detailed differences between our dataset and RaDA are as follows and summarized in Table IV.

- **Activities:** We select 6 distracted driving activities including *Smoke*, *Drink*, and *Panel*, which are observed more frequently and cause more accidents than the 5 activities identified in RaDA.
- **Restrictions of activities:** As mentioned above, we provide only minimal guidance to volunteers to prevent intentionally unusual behavior. However, in RaDA, they ask for some restrictions on activities. For instance, volunteers should use their right hand, turn their heads right when talking to a passenger, and use both hands when operating a smartphone. Such instructions may make the dataset more uniform and easier to train with, but they do not reflect typical real-world behavior.
- **Observation window size of dataset:** RaDA’s target activities can be recognized within a second to deal with their activities. However, we recommend a sufficient observation window size, at least 5 seconds, to identify more complex activities in the *ALERT* dataset; we demonstrate this in Section VI. A sufficient observation period is crucial to accurately capturing such activities’ characteristics in DAR scenario. Consequently, although both datasets provide comparable samples, the *ALERT* offers a longer total observation time.
- **Data collection environment:** In RaDA, the dashboard props up the radar installed in front of the driver, obstructing the driver’s view and leading to severe accidents. However, this setup is possible because the RaDA dataset has been collected in a simulated environment. In contrast, we position the radar on the air vent to avoid visual obstruction and collect our dataset in a real-driving environment. This setting incorporates more realistic factors, such as ground

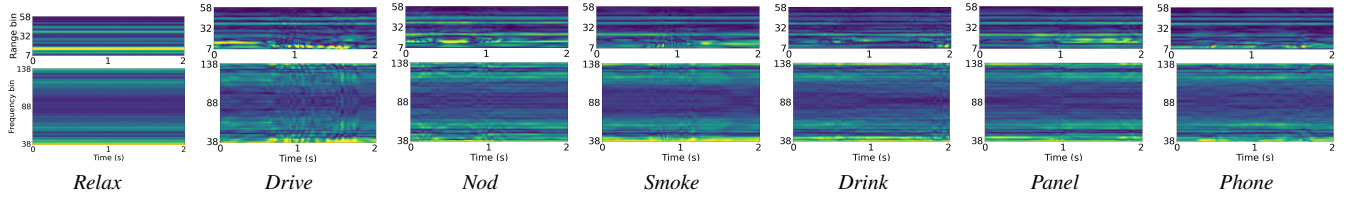


Fig. 5. Examples of range and frequency data representations for 7 activities.

and engine vibrations, and RF signal interference commonly encountered in urban areas. Consequently, the *ALERT* dataset offers a more realistic representation than RaDA.

- **Comprehensive data:** In RaDA, they only provide the single domain data. However, our *ALERT* dataset offers both range and frequency domain data, enabling the use of heterogeneous domains. Utilizing both domains contributes to extensive benchmarking experiments and evaluations. Additionally, our dataset allows manipulation according to user demands, including freely adjusting the cropping area of range and frequency and observation window size. Consequently, we can conduct extensive and varied experiments using the *ALERT* dataset, with the results evaluated and presented in Section VI.

F. Dataset and Code Availability

We publicly release the *ALERT* dataset on Figshare to facilitate further research and experimentation. Additionally, we provide the benchmarking code on GitHub, enabling users to verify benchmarking performance and offering guidance on utilizing the code with the *ALERT* dataset. The URLs for the dataset and benchmarking codes are as follows,

ALERT dataset: <https://doi.org/10.6084/m9.figshare.28244525.v3>

Benchmarking codes: <https://github.com/ALERTdataset/ALERT.git>

IV. BENCHMARKING DESIGN

To provide benchmarking performance, we design various learning models including CNN-based [36], [37], [38], [39], RNN-based [24], [22], [23], and transformer-based approaches [40], [27]. Additionally, we incorporate a multi-view learning (MVL)-based domain fusion method into all designs to demonstrate the scalability of using the *ALERT* dataset and to achieve better performance in DAR.

To further explore the most effective utilization of the *ALERT* dataset, we conduct various experiments through detailed observation. For instance, we investigate the observation time required to accurately identify DAR activities and evaluate the effects of multipath environments and frequency ranges across 8 different algorithms.

The various experiments allow us to identify optimal parameters, trends, and trade-offs specific to each algorithm. We present the results of these experiments in Section VI, providing comprehensive insights. Since the *ALERT* dataset can be customized to meet users' specific needs, sharing these experimental findings is crucial for guiding its optimal application.

A. Domain Fusion

In IR-UWB radar sensing, we primarily obtain range-time information between an object and the radar. However, relying solely on range information makes it challenging to extract distinguishing features needed to recognize similar behaviors. For example, smoking and drinking while driving are very similar activities: to do these, the driver raises and lowers their hand in a similar motion. Similarly, using a phone while driving can make it difficult to distinguish safe driving behavior. These actions exhibit only very subtle differences in range domain features. In DAR, which involves comprehensive and complex activities, failing to accurately classify similar activities can lead to decreased overall performance.

To distinguish similar activities, we implement a domain fusion method that utilizes both range and frequency domain data to capture complementary features obtained from UWB sensing. For effective fusion of range and frequency domains, it is essential to understand the feature characteristics of each domain. Each domain has distinct characteristics, outlined as follows.

The range-time domain data captures spatial information by mapping the distance of objects or activities from the sensor over time. This data is highly effective for tracking precise movements, especially rapid actions, as it can detect small shifts in position. Additionally, range-time data includes reflections from walls or objects, which can provide extra details about the surrounding environment.

We can obtain frequency-time information through a Fourier transform of the range-time data. It focuses on changes in Doppler shift over time, offering insights into the speed and direction of movement. While it provides less detail about position, frequency-time data is better suited for tracking movement velocity and patterns. Furthermore, frequency-time data is less affected by reflections, resulting in cleaner data that is easier to analyze for movement patterns. By integrating the two domains, we can make more accurate and reliable judgments about confusing labels.

In domain fusion, we leverage the various features obtained from multiple domains and concatenate each feature to classify the object. Similarly, some works [17], [19] apply the MVL-based domain fusion method to the UWB HAR for better performance. They transform the same UWB data into both range domain and frequency domain components, separately process each branch's range and frequency inputs, and then concatenate to classify the activities. The details of the domain fusion design are provided in the following, and the evaluation results using both single-domain datasets and domain fusion datasets are presented in Section VI.

B. Design for CNN-based Approach

We benchmark the performance of various CNN architectures including GoogLeNet [36], ResNet [37], DenseNet [38], and MobileNet [39]. The aforementioned algorithms are CNN-based feature extractors as depicted in Fig. 6. The range and frequency data are fed into the CNN-based feature extractor. After processing through the feature extractor, features for range and frequency are concatenated and then inputted into a classifier to recognize the activity. The classifier comprises three fully connected layers, with various dimensions tailored to the specific algorithm employed.

C. Design for RNN-based Approach

To design the RNN-based approach, we follow the conceptual framework introduced in [24], [22], [23]. Although the ALERT dataset includes sufficiently long sequences for temporal modeling, we do not adopt xLSTM [51] for benchmarking. This is because xLSTM processes individual UWB pulses sequentially, and each pulse contains only limited information. In UWB radar, meaningful activity patterns emerge only when multiple pulses are accumulated over time. To address this, we adopt the CNN+LSTM architecture that groups several pulses into short snippets, extracts spatial features from each snippet using a CNN, and then models the temporal dependencies between these snippets using an LSTM.

As depicted in Fig. 6, we split both range and frequency data into 10 snippets and use ResNet to extract features for refined input representation and dimension reduction. Subsequently, each feature extracted from the snippets is fed into an RNN-based sequential network, specifically implemented as a bidirectional LSTM model. The model outputs results from the LSTM at the last time step, which are then passed to the classifier. We set the hidden state size to 1024, considering the feature size, and utilize only one LSTM layer.

D. Design for Transformer-based Approach

For a Transformer-based approach, we utilize Vision Transformer (ViT) model [27] and Data-efficient Image Transformer (DeiT) model [40], which is a variant of ViT.

In the transformer-based approach, we adopt the early fusion method, as illustrated in Fig. 6. Since transformer-based models are computationally intensive, applying the late fusion method in a real-time DAR system is challenging. Late fusion requires two independent ViT models for each input, followed by concatenating the features extracted from their outputs, which significantly increases computational overhead.

Although late fusion achieves slightly higher accuracy compared to early fusion, we choose the early fusion method to balance both accuracy and DAR system responsiveness. The comparison between early fusion and late fusion is detailed in Section VI.

Consequently, we resize each dataset to an image size of 224×224 and assemble them into a two-channel image. The resized image is then divided into 14×14 patches. Each patch is projected into an embedding vector and combined with a positional embedding vector. These combined vectors are subsequently fed into the transformer encoder, enabling the classification of tokens derived from the transformer's output.

V. INPUT-SIZE-AGNOSTIC VISION TRANSFORMER (ISA-ViT)

Transferring the remarkable capabilities of ViTs to the UWB domain is critical for effectively classifying 2D image-like UWB datasets. However, applying a ViT pre-trained on ImageNet [52] to UWB data presents a significant challenge. In image processing, ViTs typically operate on an input size of 224×224 , divided into 16×16 patches, resulting in 196 patches (14 along both the height and width of the image). Each patch is transformed into a patch embedding vector and combined with the positional embedding vector (PEV) containing relative spatial information, forming the input to the transformer encoder.

However, in practice, the input size of UWB data cannot always be guaranteed to match the fixed size of 224×224 . This discrepancy makes it infeasible to directly apply pre-trained PEVs to UWB data. To tackle this critical issue, we propose the *ISA-ViT*, a novel approach specifically designed to adapt ViTs for UWB data and introduce the details of *ISA-ViT* as follows.

A. Preliminary Studies

The PEV is a significant parameter for capturing spatial information from the pre-trained ViT. Since the UWB data has a different size compared to image data (i.e., 224×224), applying the PEV to the UWB data requires a different way compared to image processing. As shown in Fig. 7(a), the PEVs of the 14th and 15th patches are trained to be dissimilar in ViT image tasks because of their distant spatial locations. However, if we apply these pre-trained PEVs to UWB data with different dimensions, as shown in Fig. 7(b), the 14th and 15th patches are treated as if they are far apart, despite being adjacent in reality. This mismatch can significantly degrade performance, highlighting the importance of appropriately adapting the pre-trained PEVs.

To handle non-image inputs sizes, we can consider two approaches: 1) **maintaining the pre-trained 14×14 sequence of PEVs**, or 2) **manipulating a different number and sequence of PEVs** from the pre-trained ViT for image tasks, as illustrated in Fig. 7(b).

The first approach for **maintaining pre-trained 14×14 PEVs** involves two methods: 1) *resizing the input* or 2) *adjusting the shape of the patch*. The *resizing the input* method exploits up & down-sampling techniques to make it 244×244 in size. Alternatively, we can *adjust the shape of the patch* by keeping the input data unchanged and applying patches of a different shape, rather than using the 16×16 size typically used for images. We divide the height and width of the input data by 14 to determine the patch size for both dimensions, and we add zero-padding if necessary. The common goal of both methods is utilizing the pre-trained 14×14 sequence of PEVs.

We can refer to [44] to **manipulate the PEVs**, as mentioned above the second approach. They calculate the number of patches (using 16×16 patches) along the height and width of the input data. If the number of patches in the side exceeds 14, they apply interpolation to the PEVs for height; otherwise, they

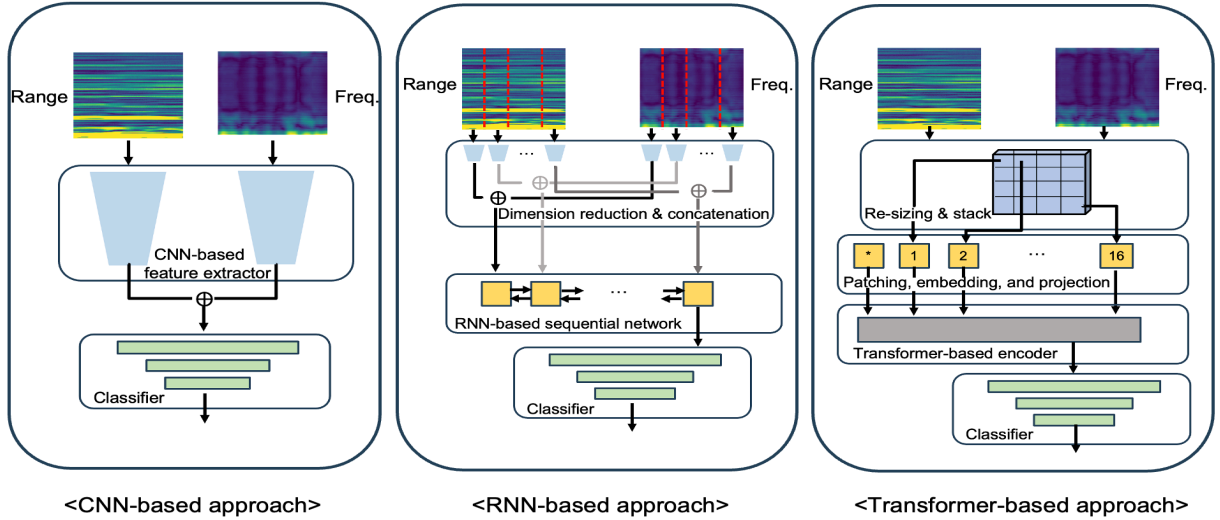
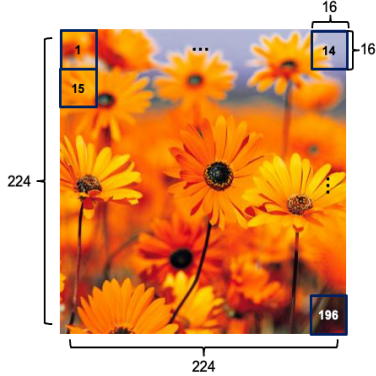
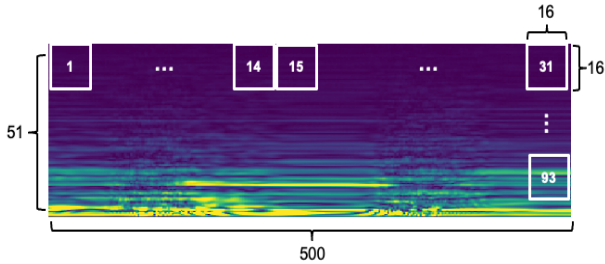


Fig. 6. Design of learning algorithms for benchmarking.



(a) Image data



(b) UWB data

Fig. 7. Application of PEVs according to input of different domain data.

use truncation. We implement *manipulating PEVs* by following the conceptual approach used in [44].

We compare each method to determine which one is the most suitable for using pre-trained PEVs. For this evaluation, we use two UWB open datasets for DAR: the *ALERT* dataset and the *RaDA* dataset [11]. Both datasets include 6–7 activities for recognizing distracted driving behaviors, such as driving, nodding, using a smartphone, etc. The *ALERT* dataset has input data samples of size 51×500 , while the *RaDA* dataset has samples of size 1024×24 .

Table V shows the average accuracy of each method for the two datasets. The methods for maintaining the pre-trained 14×14 sequence of PEVs, *resizing input* and *adjusting patch*

TABLE V
ACCURACY ACCORDING TO HANDLING METHOD FOR INPUT OF UWB DATA

Method \ Dataset	<i>ALERT</i>	<i>RaDA</i> [11]
Resizing input	52.20%	56.10%
Adjusting patch shape	43.55%	53.92%
Manipulating PEVs [44]	36.74%	49.25%

shape, demonstrate better performance than *manipulating PEVs*.

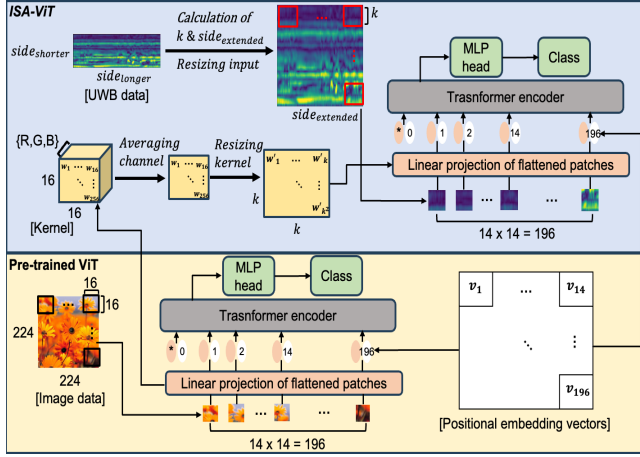
The patch sizes in the *adjusting patch shape* method are constrained to highly limited and unconventional shapes, such as wide-long or bottom-long configurations. The patches are set to 4×36 in the *ALERT* dataset and 74×2 in the *RaDA* dataset. These extreme rectangular patch shapes do not contribute positively to model performance, as they fail to capture sufficient information effectively.

The *manipulating PEVs* method underperforms due to the unique characteristics of UWB data, where the *ALERT* and *RaDA* datasets contain samples with wide or bottom-long shapes. As a result, both cutting and interpolation are applied to the pre-trained PEVs. For both datasets, we interpolate the PEVs for the width by more than twice and 4.5 times, respectively. Excessive interpolation may result in the loss of fine-grained spatial information or lead to positional embedding saturation, reducing the meaningfulness of the PEVs. Consequently, the *manipulating PEVs* struggles to adapt effectively to the shape of UWB data.

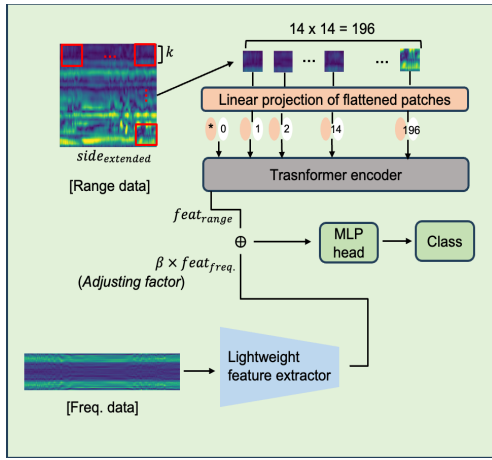
Through the preliminary studies, we observe the importance of **preserving the pre-trained 14×14 PEV sequence** for non-image input sizes. In the following section, we introduce *ISA-ViT*, a detailed method for maintaining the pre-trained sequence of PEVs, designed to effectively apply PEVs to UWB data.

B. Proposed Scheme

Our goal is to enhance the performance of DAR using IR-UWB. To achieve this, we need to design a model that effectively utilizes UWB data and develop a method that can further improve DAR performance. Therefore, we introduce *ISA-ViT* and the domain fusion method, as shown in



(a) The design of ISA-ViT



(b) The design of domain fusion

Fig. 8. Overview of the proposed scheme.

Fig. 8. The ISA-ViT enables the application of UWB data to ViT regardless of data size, while domain fusion improves DAR performance by combining information from multiple domains, resulting in better classification.

C. ISA-ViT

In the previous section, we verified that maintaining the pre-trained 14×14 sequence of PEVs yields better performance than manipulating PEVs without considering the input size. However, using simple resizing (via up & down-sampling) may result in severe information loss when the input size is much larger than the image size (i.e., 224×224). Therefore, we designed ISA-ViT with no information loss from the input data, as described in Fig. 8(a).

Our conceptual approach is as follows: UWB data commonly has a rectangular shape rather than a square (though it can also be square-shaped). First, we extend the shorter side of the input to match the size of the longer side, without any loss of information. Afterward, we calculate the patch size to divide the extended input into 14×14 patches. One important consideration is that the sides of the extended input may not be divisible by 14. Therefore, we use the following formulas

Algorithm 1 Adjustment of the size of UWB data, patch, and kernel of ISA-ViT

Parameters:

$data_{UWB}$: UWB data sample
 $num_patches$: Square root of the number of patches
 $k_{original}$: Size of the original patch
 k : Size of the new patch
 $P_{original}$: The original patch
 P_k : The new patch
 $side_{shorter/longer}$: Size of the side for data
 $size_*$: Size of *
 $weight_{kernel}(*):$ Pre-trained kernel weights of *

Input: $data_{UWB}$

1: Initialize:

$(side_{shorter}, side_{longer}) \leftarrow size(data_{UWB})$.

$size_{UWB} \leftarrow (side_{shorter}, side_{longer})$

$num_patches \leftarrow 14$

$k_{original} \leftarrow 16$

2: Calculation of k and $side_{extended}$:

$k \leftarrow \lceil \frac{side_{longer}}{num_patches} \rceil$

$side_{extended} \leftarrow num_patches \times k$

3: Resizing input:

$size_{new} \leftarrow (side_{extended}, side_{extended})$

$data_{UWB}, size_{UWB} \leftarrow$

$resize(data_{UWB}, size_{UWB} \rightarrow size_{new})$

4: Averaging channel and resizing kernel:

$weight_{kernel}(P_{original}) \leftarrow$

$channel_avg(weight_{kernel}(P_{original}))$

$weight_{kernel}(P_k), size_{kernel} \leftarrow$

$resize(weight_{kernel}(P_{original}), k_{original} \rightarrow k)$

5: Linear projection:

$output \leftarrow CNN(data_{UWB}, weight_{kernel}(P_k), size_{kernel})$

Output: Patch embedding vectors

to determine the patch size and apply resizing to adjust the input accordingly.

$$k = \min\{k \in \mathbb{Z} \mid 14 \times k \geq side_{longer}\}, \quad (2)$$

$$side_{extended} = 14 \times k, \quad (3)$$

where k is the size of the patch, $side_{longer}$ is the size of the longer side of the input, and $side_{extended}$ is the size of the side to be extended. This process ensures that there is no loss of information.

Moreover, we must consider one additional factor, which is patch embedding. After dividing the extended input into patches of size k , each patch is transformed into a patch embedding vector through linear projection using a simple CNN layer. Typically, in the image domain, a 16×16 pre-trained kernel is used, matching the patch size. In the UWB domain, we need to align not only the CNN kernel size but also the pre-trained weights of the kernel. The pre-trained CNN kernel has a 16×16 size with RGB channels, but since UWB data has only one channel, we average the weights of the RGB channels into one channel.

After that, we adjust the pre-trained CNN kernel size and weights to match the size of $k \times k$. We simply use interpolation (when $k > 16$) or average pooling (when $k < 16$) to adjust the kernel weights. Through this process, we finally combine the patch embedding vectors with the pre-trained PEVs and pass them to the transformer encoder. Fig. 8(a) and Algorithm 1 present the summarized method of ISA-ViT.

D. Domain Fusion of ISA-ViT

For domain fusion, we might initially consider using two parallel ViT models to equally extract features from range

and frequency data. However, simply fusing the features from both ViT models would make the system quite heavy as mentioned in Section IV-D. To consider both accuracy and system responsiveness, we devise the light-weight late fusion method as illustrated in Fig. 8(b). We apply *ISA-ViT* to the range data and use a lightweight feature extractor model for the frequency data. The range data is divided into $k \times k$ patches, specifically 14×14 patches, which are transformed into patch embedding vectors via linear projection. These vectors are then combined with pre-trained PEVs and processed through the transformer encoder to obtain the feature representation of the range domain data. In contrast, we pass the frequency data through the lightweight feature extractor without resizing, further reducing computational cost. This approach not only optimizes system efficiency but also places greater emphasis on the range domain data due to its distinctive feature characteristics.

The reason we focus more on range domain data is that it provides essential information about behaviors. When identifying a driver’s actions while driving, range information is highly valuable, as it helps in understanding the size and nature of behaviors. For example, by utilizing range information, we can distinguish whether the driver is holding a phone in front of their body to use it or bringing a cigarette to their mouth to smoke. While frequency information offers insights into speed changes and movement direction, it is insufficient on its own to accurately identify the driver’s behavior. For instance, even if the speed remains constant, frequency data alone cannot reveal whether the driver is dozing off or actively focused on driving. Consequently, we place greater emphasis on range domain features and less on frequency domain features.

We primarily utilize features extracted from the range domain, with frequency domain data providing supplementary information. Instead of concatenating frequency features at the same ratio as range features, we apply an adjusting factor β to balance the frequency domain features before concatenation. The rationale for this approach is that range and frequency data do not always complement each other positively in domain fusion. This method ensures that the contribution from the frequency domain is balanced and does not overpower the more informative range domain features. We can determine the optimal value of the adjusting factor β through the training phase.

Our domain fusion approach enhances DAR performance by effectively combining the unique characteristics of the range and frequency domains, addressing the limitations of classification performance when using the single domain. Detailed results from our proposed scheme are presented in the Section VI.

VI. EVALUATIONS

A. Experimental Settings

Benchmarking. We leverage a system running Ubuntu 22.04.5 LTS, equipped with an Intel® Core™ i9-12900K CPU and a single NVIDIA GeForce RTX A6000 GPU with 49 GB of memory in our experiments. The software environment included Python 3.10.12 and CUDA 11.5.119 with CUDA support.

We conduct extensive experiments using the *ALERT* dataset, which comprises 7 activities with 10,220 samples collected from 9 participants. The observation window is set to 5 seconds, with 8–58 range bins and 89–178 frequency bins in the range and frequency domain data.

Using the *ALERT* dataset, we benchmark several learning algorithms, including GoogLeNet [36], ResNet [37], DenseNet [38], MobileNet [39], an RNN-based model [24], [22], [23] (denoted as RNN), and transformer-based models such as DeiT [40] and ViT [27]. Each model is implemented as described in Section IV.

To ensure adequate fine-tuning, we train the models for 30 epochs, using a learning rate between 0.00001 and 0.0001 to achieve convergence of the training loss for each algorithm. Cross-entropy loss is employed as the loss function, and the Adam optimizer is used for all models.

Evaluation of *ISA-ViT*. We thoroughly evaluate the performance of DAR using *ISA-ViT* and the proposed domain fusion method. To conduct extensive experiments, we employ the *ALERT* dataset and *RaDA* dataset [11] which are open dataset leveraging IR-UWB to detect driver distraction activities.

The *ALERT* dataset not only offers comprehensive data recorded in real driving environments but also provides manipulable data tailored to users’ specific needs. We utilize both range-time and frequency-time domain data from the *ALERT* dataset to capture detailed features across different modalities.

The *RaDA* dataset comprises 10,406 samples across 6 activities (i.e., driving, autopilot, sleeping, driving while using a smartphone, smartphone use, and talking to a passenger) in a simulated environment. Since the *RaDA* dataset provides only single domain data, we cannot apply it to the domain fusion method and instead primarily use it to evaluate the impact of *ISA-ViT*.

For model training, we strictly separate the training and testing datasets; the testing dataset consists of data from drivers who were not seen during the training phase. We employ a learning rate as 0.00001 to ensure convergence the training loss. The base model is a ViT pre-trained on ImageNet [52], which uses embedding vectors of size 1,024. We fine-tune the model over 30 epochs, optimizing it with cross-entropy loss and the Adam optimizer to ensure robust performance.

B. Benchmarking Results for *ALERT* Dataset

1) **Benchmarking of learning algorithms:** For rigorous evaluation, we conduct benchmark tests using an unseen dataset during the training phase. In these experiments, we fine-tune pre-trained models, leveraging the pre-trained models’ great capabilities for feature extraction effectively to the UWB domain.

To identify a suitable model for UWB DAR, we first present the average accuracy of each algorithm. We select four unseen testers and perform leave-one-out cross-validation to calculate their average accuracy. Fig. 9(a) shows the average accuracy of various learning algorithms.

CNN-based approaches achieve an accuracy range of 61.37–71.22%, outperforming both RNN-based and transformer-based approaches. The underperformance of the RNN-based

approach stems from the lack of a pre-trained LSTM model. While it leverages pre-trained models for snippet feature extraction, the sequential LSTM model itself is not pre-trained, which limits its overall effectiveness.

Although transformer-based approaches are state-of-the-art models, they also fail to outperform CNN-based methods due to challenges outlined in Section V. While transformers excel in extracting features for image-based tasks, they require resizing UWB data and adapting pre-trained PEVs. Without addressing these issues, transformer-based approaches cannot fully leverage their potential in the UWB domain.

In contrast, the proposed *ISA-ViT* overcomes these challenges by resizing UWB data without information loss and adapting the pre-trained PEVs to the resized data. As a result, *ISA-ViT* achieves the highest accuracy of 76.28%, demonstrating its superior performance.

Along with the accuracy, other important metrics to consider are the precision and recall for each activity. High precision or recall does not always guarantee good accuracy, but they are valuable metrics for evaluating classification performance. Table VI presents the precision and recall values for each activity across the evaluated learning algorithms. The underlined values in Table VI represent the fluctuations in precision and recall for each activity. The variance of these metrics is particularly important as it reflects the model’s ability to maintain stable classification performance across different activities. Fig. 9(b) the mean and deviation of activities for each metric by algorithms. As shown in the figure, other algorithms often exhibit significant deviations; the *ISA-ViT* demonstrates a generally stable variance, ensuring more consistent classification performance for each activity.

C. Ablation Studies for ALERT dataset

We conduct various experiments to identify the optimal parameters, trends, and trade-offs for each algorithm when utilizing the *ALERT* dataset.

1) **Analysis for manipulation of data size:** We conduct experiments with varying observation window sizes, range bins, and frequency bins of *ALERT* dataset to determine the optimal data size for accurately capturing activities.

As shown in Fig. 10(a), we observe that accuracy improves as the observation window increases. Specifically, window sizes of 1 and 2 seconds do not provide sufficient performance due to the limited time available to accurately identify activities. In contrast, window sizes of 5 and 10 seconds offer adequate time to enhance performance. However, longer observation windows also lead to increased inference time and higher computational costs. Therefore, it is essential to consider a balance between observation window size, system responsiveness, and practical computational efficiency.

In Fig. 10(b), we compare the total range bins (about 9 m) with a cropped range bins (< 2.7 m) to examine the effects of long-delayed multi-path signals. The ability to effectively extract features from long-delayed multi-path signals varies depending on the structure of the algorithm. However, except for ResNet, all algorithms perform better with cropping applied. Although multipath signals may occasionally

carry useful information about the surrounding environment—such as the presence of passengers or the type of vehicle—they generally act as noise for most algorithms. Consequently, applying cropping is beneficial for most algorithms.

Additionally, we analyze lower (< 375 MHz), higher (375–750 MHz), and total frequency areas to determine which segments best capture the movement characteristics associated with various activities. In frequency domain, distinct results emerge for each algorithm, with the ability of feature extraction varying depending on the algorithm used. Consequently, these results should guide the selection of an appropriate algorithm.

2) **Analysis for the number of shots:** We present the impact of varying the number of shots on a few-shot adaptation. To obtain a few shot samples, the driver has to capture the activities, which can be burdensome; however, this occurs only once when the system is initially operated. For the few-shot adaptation phase, we utilize various number of shot samples and 10 epochs adaptation, which are enough to fit the model to a driver. As shown in Fig. 10(c), the accuracy increases when all models’ number of shots increases. We observe that even with the addition of only about 5 shots, the accuracy gain is significant. In particular, when applying 30 shots to *ISA-ViT*, it exhibits a maximum performance of 91.75%.

However, we spend 50, 100, and 150 seconds per activity to obtain 10, 20, and 30 shots, respectively. It can be a burden to the drivers although we collect only once at the first time. We should increase the number of shots in perspective of accuracy but decrease the number of shots to reduce the driver’s burden. Thus, we should select a moderate number of shots, considering the balance between accuracy and burdens.

3) **Analysis for the input data domain:** The *ALERT* dataset provides both range and frequency domain data, enabling users to select the data domain for their specific needs. To evaluate the impact of each domain on performance, we assessed the use of range only, frequency only, and a combination of both domains, with the results illustrated in Fig. 10(d).

In CNN-based approaches, except for MobileNet, algorithms perform better when using the frequency domain compared to the range domain. Conversely, in RNN-based, transformer-based, and *ISA-ViT* models, using the range domain yield better results than using frequency domain.

Interestingly, using both domains does not consistently improve performance. Except for RNN and DeiT, all algorithms demonstrate improved performance when using domain fusion compared to using a single domain. While combining two domains generally enhances performance through complementary synergy, this is not always true for all algorithms. These results indicate that the optimal domain should be chosen based on the characteristics of the specific algorithm.

4) **Analysis for the range-Doppler data domain:** As shown in Fig. 2, the *ALERT* dataset manipulates UWB radar sensing data into range-time and frequency-time domains. One of the key contributions of the *ALERT* dataset is that users can flexibly manipulate the data according to their specific needs. To demonstrate this data flexibility, we conduct an experiment using range-Doppler domain data. The range-Doppler format is used in datasets such as RaDA, and the *ALERT* dataset also supports this format. Users can easily perform this conversion

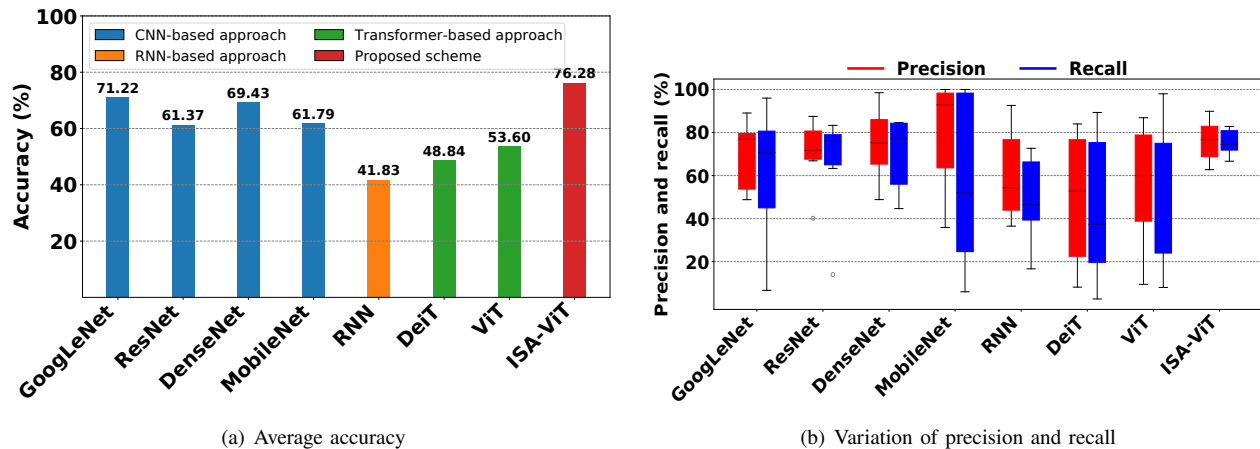


Fig. 9. Benchmarking results for overall performance: accuracy, precision, and recall.

TABLE VI
BENCHMARKING [PRECISION / RECALL] OF LEARNING ALGORITHMS

Alg. Act.	GoogLeNet	ResNet	DenseNet	MobileNet	RNN	DeiT	ViT	ISA-ViT
<i>Drive</i>	89.07 / 70.66	84.72 / 81.33	90.71 / 84.66	65.17 / 97.33	68.62 / 46.66	78.01 / 73.33	86.88 / 35.33	68.51 / 79.76
<i>Relax</i>	80.00 / 34.66	76.68 / 83.33	72.35 / 59.33	61.98 / 100.0	84.72 / 40.66	75.32 / 77.33	72.41 / 98.00	89.87 / 69.50
<i>Nod</i>	50.20 / 82.00	66.86 / 76.66	58.29 / 77.33	96.66 / 38.66	45.41 / 72.66	52.83 / 37.33	85.29 / 38.66	69.12 / 82.83
<i>Drink</i>	48.81 / 96.00	68.34 / 63.33	75.23 / 52.66	100.0 / 6.00	92.59 / 16.66	84.00 / 28.00	60.00 / 54.00	76.64 / 82.00
<i>Phone</i>	79.04 / 55.33	71.69 / 76.00	81.29 / 84.00	92.85 / 52.00	42.46 / 71.33	34.35 / 89.33	41.26 / 96.00	81.50 / 74.17
<i>Smoke</i>	76.92 / 6.66	40.16 / 66.66	48.84 / 84.66	35.90 / 99.33	36.50 / 61.33	10.62 / 11.33	9.45 / 12.66	62.75 / 66.67
<i>Panel</i>	57.21 / 79.33	87.5 / 14.00	98.52 / 44.66	100.0 / 10.66	54.28 / 38.00	8.16 / 2.66	36.36 / 8.00	84.34 / 74.50

using our provided script (ALERT_makeDataset.py) available in the public repository (<https://github.com/ALERTdataset/ALERT.git>).

As shown in Fig. 11, CNN- and RNN-based methods using range-Doppler inputs do not outperform their counterparts using domain fusion inputs shown in Fig. 9(a). In contrast, ViT-based models, including DeiT and ViT, achieve better performance when using range-Doppler data compared to domain fusion inputs.

This difference can be explained by how the models handle the input data. CNNs and RNNs can directly process UWB radar inputs without resizing. In contrast, DeiT and ViT require resizing the input to 224×224 , causing a significant reduction in resolution. During domain fusion, the time resolution is cut by more than half in both the range-time and frequency-time domains. Similarly, converting to the range-Doppler domain reduces the Doppler resolution by about half. However, we observe that the loss of time resolution has a more critical impact on these models than the loss of Doppler resolution.

Our proposed model, *ISA-ViT*, is built on a ViT backbone but incorporates a resizing strategy that preserves the original information without loss. This design enables *ISA-ViT* to achieve better performance compared to other models when using input from the Doppler range domain. Furthermore, *ISA-ViT* employs a complementary fusion technique that effectively integrates range and frequency information. As demonstrated in Fig. 9(a), this approach leads to improved performance compared to using range-Doppler data alone.

5) *Comparison of early fusion and late fusion*: Unlike CNN-based and RNN-based approaches, transformer-based approaches have possible design choices for domain fusion,

early fusion and late fusion. However, we applied the early fusion method in Section IV. To verify the effectiveness of early fusion, we compare the accuracy and computational cost of early fusion and late fusion as shown in Fig. 12.

Fig. 12 shows the performance of ViT. While late fusion, which extracts features using separate ViTs, achieves approximately 3% higher accuracy than early fusion, its computational cost is nearly double. Although early fusion may yield slightly lower accuracy, it provides significant benefits in terms of computational efficiency. In late fusion, each input is processed by a separate ViT, and the resulting features are combined and passed to a classifier. Since ViTs are computationally expensive, using two parallel ViTs imposes a heavy system burden. Therefore, we adopt early fusion for the transformer-based approach.

D. Data Verification

To confirm that the *ALERT* dataset is suitable for training models, we indirectly verify it by analyzing its feature distribution. Typically, we use visualization of feature distributions to verify models; but, if we can confirm well-distributed features when we pass through the *ALERT* dataset to the verified model, we can verify our dataset. Fig. 13 illustrates the feature distribution of each algorithm using t-distributed stochastic neighbor embedding (T-SNE). We reduce the dimension of features from the penultimate layer of each model.

All models exhibit differentiation of features. Overall, this analysis confirms that the *ALERT* dataset is meaningfully assembled. Note that the results only verify whether our data can be used well enough for the models, so there is no relationship between overall accuracy. Accuracy may vary

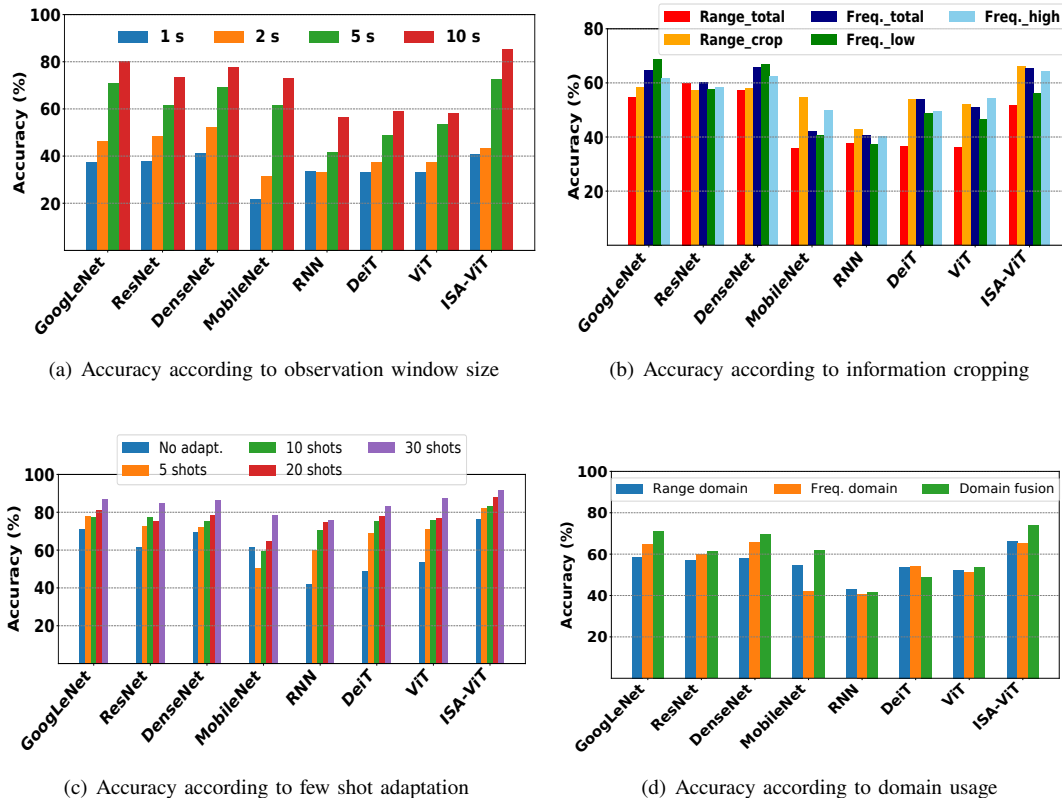


Fig. 10. Ablation studies for *ALERT* dataset.

depending on the distribution of testers. Thus, the results guarantee training accuracy, not testing accuracy.

E. Evaluations of ISA-ViT

1) **Overall performance:** We evaluate the overall performance of DAR using UWB data. Our proposed model, *ISA-ViT*, is designed to handle various sizes of UWB data, making it adaptable to different data configurations. Furthermore, we incorporate a domain fusion algorithm to enhance the overall performance of DAR, enabling our system to leverage features from multiple domains for better classification results. The fusion of range-time and frequency-time domain features allows the model to capture more intricate patterns of driver activities, which are often missed by single-domain approaches. This multi-domain synergy significantly improves the accuracy and robustness of the system across diverse driving scenarios.

Fig. 14 shows the overall performance of the proposed scheme; Fig. 14(a) displays the average accuracy. We analyze accuracy from two perspectives; one considers both service-related aspects and safety driving, while the other focuses solely on accuracy from an extreme safety driving oriented perspective.

We refer to the classification accuracy (76.28%), F1 score in Table VII, and confusion matrix in Fig. 14(b) to analyze the model's accuracy from both safety and service perspectives. The classification accuracy reflects the model's ability to categorize all activities within our proposed framework. The

precision and recall of each activity indicate the safety and service factors. If the recall for *Drive* is low, the system may trigger false alarms, potentially interrupting the driving experience and reducing overall service quality. While false alarms may be frustrating from a service perspective, they do not pose significant safety risks. However, the precision for *Drive* is directly linked to safety. Low precision could indicate that other potentially dangerous activities, such as using a smartphone, smoking, nodding are incorrectly classified as driving. Thus, we should refer to classification accuracy and F1 score together to analyze the accuracy in perspectives of safety and service.

Given that safe driving is more critical than general classification performance, **high accuracy in detecting distracted driving is essential**. In our case, the system should ensure that no activity other than *Drive* is allowed while the vehicle is in motion. This requirement is crucial for maintaining safety, as identifying activities such as using a smartphone or smoking while driving is vital to preventing distractions that could lead to accidents. To this end, we focus on accuracy specifically related to the detection of distracted activities. While service-related aspects were not considered, achieving an accuracy of 97.35% demonstrates a substantial contribution to enhancing road safety.

2) **Impact on resizing method:** To evaluate *ISA-ViT*, we conduct experiments with several resizing methods for the *ALERT* and *RaDA* datasets. We have already verified that maintaining the 14×14 sequence of pre-trained PEVs yields

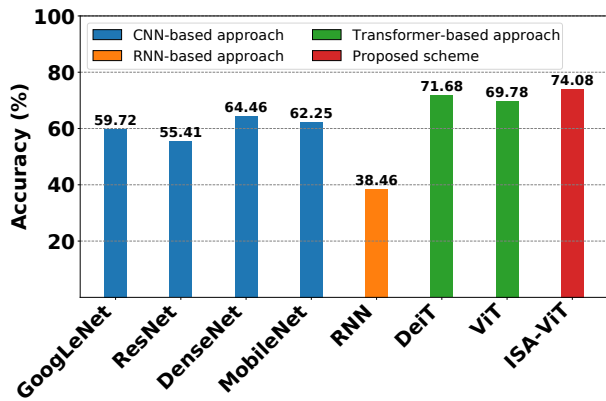


Fig. 11. Average accuracy using range-Doppler domain of *ALERT*.

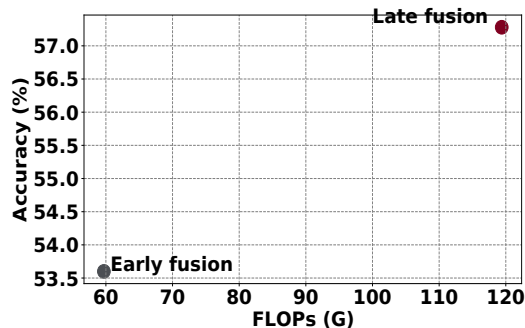


Fig. 12. Accuracy and computational cost comparison of early fusion with late fusion in transformer-based approach.

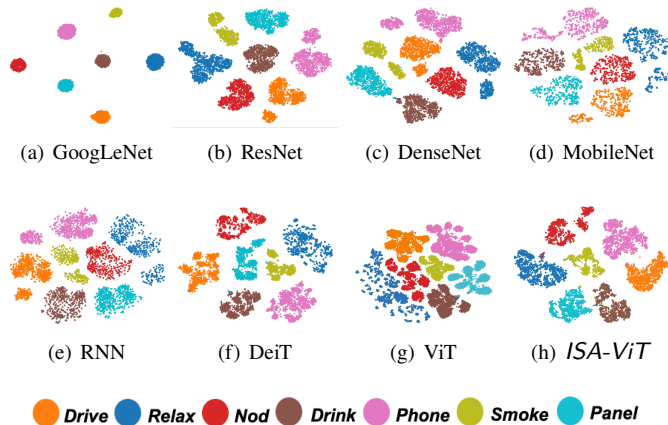


Fig. 13. T-SNE based feature visualization of learning algorithms.

better performance than manipulating them in Section V. Therefore, we only compare methods that maintain pre-trained PEVs.

Fig. 15 compares the average accuracy of different resizing methods. The blue bar represents the simple resizing method, which applies basic up- and down-sampling to reshape the data to 224×224 . The green bars show CNN-based methods, which first use early CNN layers to extract local features from UWB data, then apply up- and down-sampling to adjust the feature size to 224×224 . *GoogLeNet_1* and *GoogLeNet_2* use the first and second inception modules of *GoogLeNet*, while *ResNet_1* and *ResNet_2* use the first and second blocks of *ResNet*.

For the *ALERT* dataset, as shown in Fig. 15(a), using CNN-

TABLE VII
PRECISION, RECALL, AND F1 SCORE FOR EACH LABEL

	<i>Drive</i>	<i>Relax</i>	<i>Nod</i>	<i>Drink</i>	<i>Phone</i>	<i>Smoke</i>	<i>Panel</i>
Precision	68.51	89.87	69.12	76.64	81.50	62.75	84.34
Recall	79.76	69.50	82.83	82.00	74.17	66.67	74.50
F1 score	73.71	78.38	75.36	79.23	77.66	64.65	79.12

TABLE VIII
COMPARISON OF PRECISION, RECALL, AND F1 SCORE BEFORE/AFTER DOMAIN FUSION

Before	<i>Relax</i>	<i>Drive</i>	<i>Nod</i>	<i>Drink</i>	<i>Phone</i>	<i>Smoke</i>	<i>Panel</i>
Precision	87.56	57.19	58.73	61.64	69.24	76.54	78.69
Recall	56.33	85.24	75.67	77.67	70.17	51.67	56.00
F1 score	68.56	68.45	66.13	68.73	69.70	61.69	65.43
After	<i>Relax</i>	<i>Drive</i>	<i>Nod</i>	<i>Drink</i>	<i>Phone</i>	<i>Smoke</i>	<i>Panel</i>
Precision	89.87	68.51	69.12	76.64	81.50	62.75	84.34
Recall	69.50	79.76	82.83	82.00	74.17	66.67	74.50
F1 score	78.38	73.71	75.36	79.23	77.66	64.65	79.12

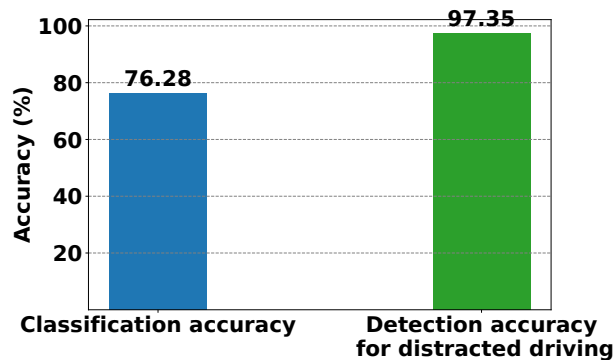
based resizing approaches outperforms simple resizing, as they minimize information loss by using feature extraction instead of simple down-sampling. However, *ISA-ViT* retains the raw UWB data information without any loss, leading it to outperform the other methods.

For the *RaDA* dataset, we use only *ResNet_2* in the CNN-based method since its input size is 1024×24 . When using only a single *ResNet* block, the data size becomes 512×12 , resulting in approximately half down-sampling, which increases the likelihood of information loss. Therefore, passing the data through two blocks and then resizing it to fit 224 is necessary to minimize information loss. Additionally, in the case of *GoogLeNet*, using the inception module leads to a significant reduction in size, requiring additional padding, making it unsuitable for our experiments.

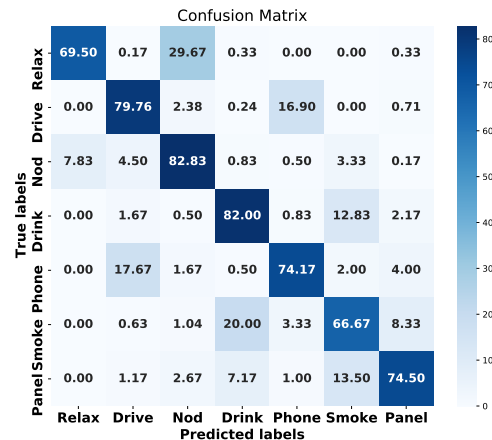
As shown in Fig. 15(b), simple resizing outperforms the CNN-based method in the *RaDA* dataset. Due to the dataset's characteristics, the key information is centered within the sample, so when CNN-based methods are applied, the features cover only a small portion of the sample. Thus, simple resizing performs better than the CNN-based method. However, *ISA-ViT* outperforms all methods due to its ability to resize without information loss.

Through this ablation study, we demonstrate that, for CNN-based approaches, the number of layers the input passes through depends on the input size. However, *ISA-ViT* can be applied to any input size without such considerations, offering greater flexibility and adaptability.

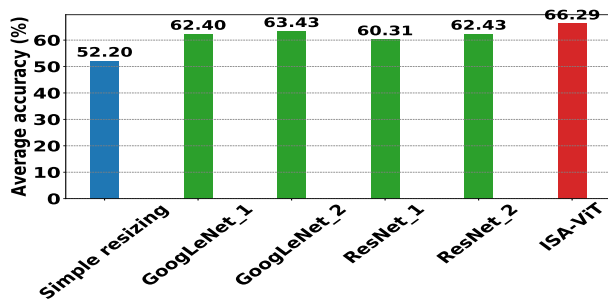
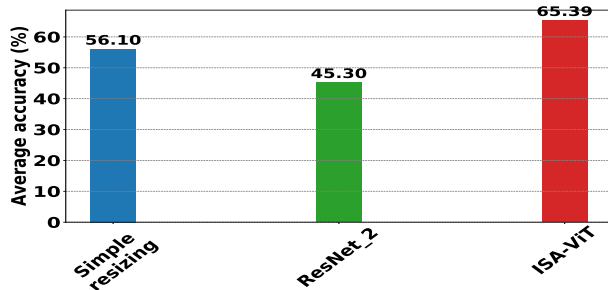
3) **Impact on domain fusion:** To enhance the performance of DAR using UWB, we jointly exploit the range domain and the frequency domain of UWB data. As shown in Fig. 16, using only the range domain and the frequency domain achieves accuracy of 66.29% and 65.45%, respectively. The range domain performs slightly better than the frequency domain in DAR. However, since each domain classifies data based on its unique characteristics, they often provide different predictions for the same input. Therefore, combining and using the feature information from both domains jointly can lead to improved results. Consequently, the domain fusion algorithm achieves an accuracy of 76.28%.



(a) Overall accuracy



(b) Confusion matrix of proposed scheme

Fig. 14. Experimental results for *ISA-ViT* performance.(a) Using *ALERT* dataset(b) Using *RaDA* datasetFig. 15. Accuracy comparison for resizing methods: simple resizing (using up- and down-sampling), GoogLeNet_x (using xth inception modules and up- and down-sampling), ResNet_x (using xth blocks and up- and down-sampling).

Moreover, Fig. 16 illustrates the accuracy impact of the trained adjusting factor β for frequency features. Before training the adjusting factor β , we achieve a performance of 74.02% with range and frequency features at an equal ratio. However, after jointly training β and applying it to domain fusion, we observe an accuracy of 76.28%. This confirms that it is crucial not merely to combine range and frequency features, but to balance them appropriately for optimal fusion.

The detailed performance enhancements are presented in Table VIII, which shows the precision, recall, and F1 score for each activity before and after applying domain fusion. For

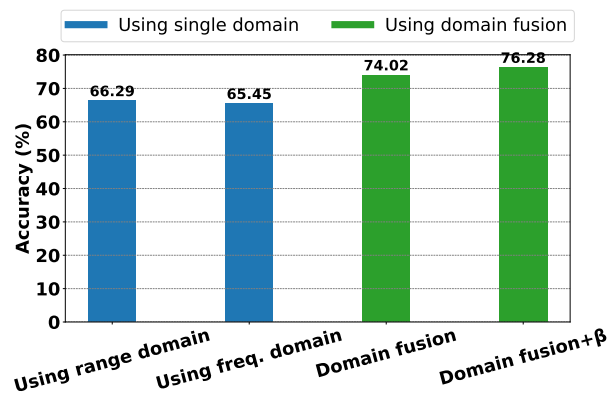


Fig. 16. Accuracy results for domain fusion.

all activities, the F1 scores improve after domain fusion is applied. These improvements demonstrate that by combining information from different domains, the model can more accurately distinguish similar activities that were previously easily confused. While precision and recall tendencies of some activities may vary, the overall improvement in F1 scores indicates a well-balanced trade-off between precision and recall, resulting in strong performance. The enhanced F1 scores for each activity after domain fusion confirm the model's improved ability to recognize a variety of activities more accurately. Through these experiments, we verify that using the domain fusion algorithm helps resolve conflicts between labels and enables more precise classification.

4) **Comparison with CNN models:** We compare the performance of ViT and CNN models with *ISA-ViT*. Although standard ViT is a state-of-the-art model for vision tasks, directly applying raw UWB data without resizing leads to poor recognition accuracy, as mentioned in the Section V-A. To enable fair comparison, we apply the simple resizing method to the UWB data before inputting it into ViT and compare its performance with CNN models and *ISA-ViT*.

In the *ALERT* dataset, as shown by the blue bars in

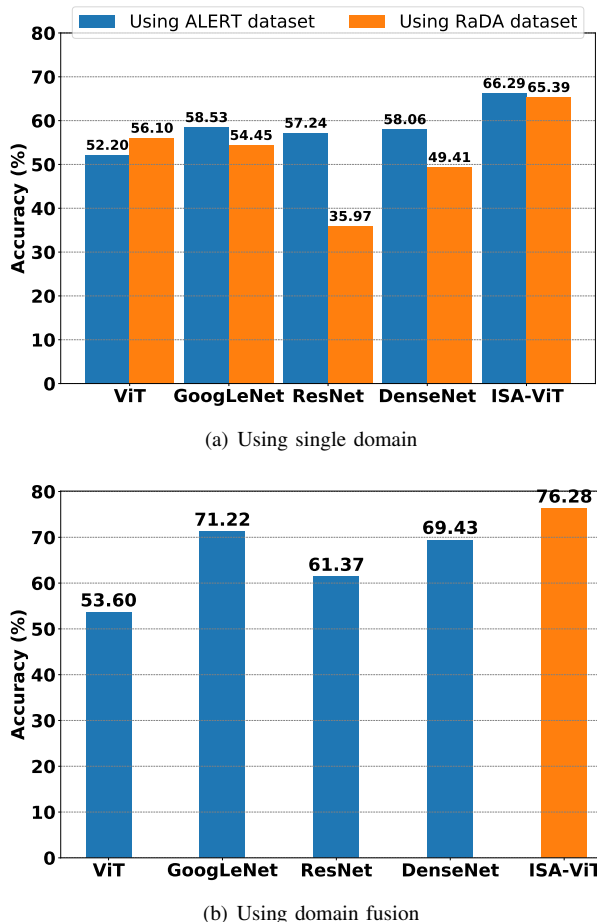


Fig. 17. Accuracy comparison with CNN models.

Fig. 17(a), CNN models outperform ViT. This is because the simple resizing approach causes significant information loss, depending on the input size. For the *ALERT* dataset, nearly half of the data information is lost during resizing. In contrast, *ISA-ViT* achieves higher performance than CNNs by allowing ViT to process data without information loss, regardless of input size.

However, the *RaDA* dataset, shown by the orange bars in Fig. 17(a), displays a different trend. This dataset has a size of 1024×24 , forming a tall and narrow shape with most key features located near the center. In this case, simple resizing, which increases the horizontal dimension, helps ViT better capture structural patterns, leading to better performance than CNN-based methods¹. Nonetheless, *ISA-ViT* achieves the best performance overall, as it resizes data without information loss.

These results show that performance varies depending on the data characteristics and model architecture. Still, *ISA-ViT* consistently provides the best performance across both datasets by preserving data information during resizing and effectively leveraging pre-trained PEVs.

For the comparison with domain fusion of CNN models as shown in Fig. 17(b), we only use the *ALERT* dataset since

¹The better performance of CNN-based methods is due to the use of simple resizing for ViT. When we apply standard ViT to raw UWB data without resizing, the model fails to train properly on both the *ALERT* and *RaDA* datasets, resulting in less than 20% accuracy.

RaDA provides only the single domain data. We apply the same CNN models in parallel as feature extractors, passing both range and frequency domain data through each model. We then concatenate the features from each model and pass the concatenated features to the classifier. Here, we use the adjusting factor β for the frequency domain, consistent with the domain fusion method of *ISA-ViT*. Therefore, we also train β to achieve the best accuracy in the domain fusion of all CNN models. In a fair comparison, using the best performance of each method, our proposed scheme outperforms the CNN models.

VII. CONCLUSION

This study addresses the critical issue of distracted driving, a significant contributor to traffic accidents worldwide, by proposing a novel Driver Activity Recognition (DAR) framework utilizing IR-UWB radar. IR-UWB technology overcomes the limitations of traditional methods, including privacy concerns, noise sensitivity, and interference issues. Despite its potential, two key challenges are identified: the lack of comprehensive datasets reflecting real-world driving conditions and the difficulty of adapting state-of-the-art models, such as Vision Transformers (ViTs), to process non-image UWB data.

To address these challenges, we developed the *ALERT* dataset, a large-scale collection of 10,220 samples representing seven diverse distracted driving activities in real-world driving environments. This dataset includes both range and frequency domain data, enabling robust experimentation and setting a new benchmark for realistic DAR studies. Additionally, we introduced *ISA-ViT*, a tailored model designed to seamlessly process UWB data of varying input sizes by resizing data without loss and adapting pre-trained positional embedding vectors. The integration of domain fusion further enhances performance by combining complementary features from the range and frequency domains.

Through extensive experiments, we analyzed the optimality, trends, and trade-offs of the *ALERT* dataset parameters across algorithms and demonstrated the effectiveness of the proposed framework. *ISA-ViT* achieved a classification accuracy of 76.28% and a distracted driving detection accuracy of 97.35%. These results underscore the transformative potential of UWB radar and transformer-based models for advancing DAR research.

By making the *ALERT* dataset publicly available and providing comprehensive benchmarking results, this study lays a foundation for future research, fostering innovation and collaboration within the DAR community. Ultimately, the proposed methods and dataset aim to contribute to safer road environments by mitigating distracted driving incidents.

REFERENCES

- [1] W. H. Organization, *Global status report on road safety 2018*. World Health Organization, 2019.
- [2] NHTSA, “Distracted driving,” <https://www.nhtsa.gov/risky-driving/distracted-driving>, [Online; accessed 20-June-2024].
- [3] Ohn-Bar *et al.*, “Head, eye, and hand patterns for driver activity recognition,” in *2014 22nd international conference on pattern recognition*. IEEE, 2014, pp. 660–665.

- [4] Kavi *et al.*, “Multiview fusion for activity recognition using deep neural networks,” *Journal of Electronic Imaging*, vol. 25, no. 4, pp. 043 010–043 010, 2016.
- [5] Xie *et al.*, “Hearsnoking: Smoking detection in driving environment via acoustic sensing on smartphones,” *IEEE Transactions on Mobile Computing*, vol. 21, no. 8, pp. 2847–2860, 2021.
- [6] Y. Xie *et al.*, “D3-guard: Acoustic-based drowsy driving detection using smartphones,” in *IEEE INFOCOM 2019-IEEE Conference on Computer Communications*. IEEE, 2019, pp. 1225–1233.
- [7] X. Xie *et al.*, “Wireless csi-based head tracking in the driver seat,” in *Proceedings of the 14th International Conference on Emerging Networking Experiments and Technologies*, 2018, pp. 112–125.
- [8] Jia *et al.*, “Wifind: Driver fatigue detection with fine-grained wi-fi signal features,” *IEEE Transactions on Big Data*, vol. 6, no. 2, pp. 269–282, 2018.
- [9] Bai *et al.*, “Widrive: Adaptive wifi-based recognition of driver activity for real-time and safe takeover,” in *2019 IEEE 39th International Conference on Distributed Computing Systems (ICDCS)*. IEEE, 2019, pp. 901–911.
- [10] Y. Bai *et al.*, “Carin: Wireless csi-based driver activity recognition under the interference of passengers,” *Proceedings of the ACM on Interactive, Mobile, Wearable and Ubiquitous Technologies*, vol. 4, no. 1, pp. 1–28, 2020.
- [11] Brishtel *et al.*, “Driving activity recognition using uwb radar and deep neural networks,” *Sensors*, vol. 23, no. 2, p. 818, 2023.
- [12] Hu *et al.*, “Blinkradar: non-intrusive driver eye-blink detection with uwb radar,” in *2022 IEEE 42nd International Conference on Distributed Computing Systems (ICDCS)*. IEEE, 2022, pp. 1040–1050.
- [13] Bai *et al.*, “Fusing wifi signals and camera for driver activity recognition based on deep learning,” in *2022 IEEE 19th International Conference on Mobile Ad Hoc and Smart Systems (MASS)*. IEEE, 2022, pp. 18–26.
- [14] S. Hwang, Y. Kim, S. Kim, S. Bahk, and H.-S. Kim, “Upcycling: Semi-supervised 3d object detection without sharing raw-level unlabeled scenes,” in *Proceedings of the IEEE/CVF International Conference on Computer Vision (ICCV)*, October 2023, pp. 23 351–23 361.
- [15] Y. Kim, S. Hwang, H.-S. Kim, and S. Bahk, “Concretizer: Model inversion attack via occupancy classification and dispersion control for 3d point cloud restoration,” in *The Thirteenth International Conference on Learning Representations (ICLR)*, April 2025.
- [16] FIRa, “UWB Technology Comparison,” <https://www.firaconsortium.org/discover/comparison>, [Online; accessed 01-July-2024].
- [17] Chen *et al.*, “Rf-based human activity recognition using signal adapted convolutional neural network,” *IEEE Transactions on Mobile Computing*, vol. 22, no. 1, pp. 487–499, 2021.
- [18] Shao *et al.*, “Human motion classification based on range information with deep convolutional neural network,” in *2017 4th International Conference on Information Science and Control Engineering (ICISCE)*. IEEE, 2017, pp. 1519–1523.
- [19] Piriyaajakonkij *et al.*, “Sleepnet: Multi-view learning for sleep postural transition recognition using uwb,” *IEEE Journal of Biomedical and Health Informatics*, vol. 25, no. 4, pp. 1305–1314, 2020.
- [20] Xu *et al.*, “Uhead: Driver attention monitoring system using uwb radar,” *Proceedings of the ACM on Interactive, Mobile, Wearable and Ubiquitous Technologies*, vol. 8, no. 1, pp. 1–28, 2024.
- [21] Han *et al.*, “Ir-uwb sensor based fall detection method using cnn algorithm,” *Sensors*, vol. 20, no. 20, p. 5948, 2020.
- [22] Maitre *et al.*, “Recognizing activities of daily living from uwb radars and deep learning,” *Expert Systems with Applications*, vol. 164, p. 113994, 2021.
- [23] Noori *et al.*, “Ultra-wideband radar-based activity recognition using deep learning,” *IEEE Access*, vol. 9, pp. 138 132–138 143, 2021.
- [24] Maitre *et al.*, “Fall detection with uwb radars and cnn-lstm architecture,” *IEEE journal of biomedical and health informatics*, vol. 25, no. 4, pp. 1273–1283, 2020.
- [25] Li *et al.*, “Human activity recognition using ir-uwb radar: A lightweight transformer approach,” *IEEE Geoscience and Remote Sensing Letters*, 2023.
- [26] Zhao *et al.*, “Distributed radar-based human activity recognition using vision transformer and cnns,” in *2021 18th European Radar Conference (EuRAD)*. IEEE, 2022, pp. 301–304.
- [27] Dosovitskiy *et al.*, “An image is worth 16x16 words: Transformers for image recognition at scale,” *arXiv preprint arXiv:2010.11929*, 2020.
- [28] Han *et al.*, “A survey on vision transformer,” *IEEE transactions on pattern analysis and machine intelligence*, vol. 45, no. 1, pp. 87–110, 2022.
- [29] Khan *et al.*, “Transformers in vision: A survey,” *ACM computing surveys (CSUR)*, vol. 54, no. 10s, pp. 1–41, 2022.
- [30] Ruan *et al.*, “Vision transformers: state of the art and research challenges,” *arXiv preprint arXiv:2207.03041*, 2022.
- [31] Li *et al.*, “Human activity recognition using ir-uwb radar: A lightweight transformer approach,” *IEEE Geoscience and Remote Sensing Letters*, 2023.
- [32] Zhao *et al.*, “Distributed radar-based human activity recognition using vision transformer and cnns,” in *2021 18th European Radar Conference (EuRAD)*. IEEE, 2022, pp. 301–304.
- [33] Lai *et al.*, “Vision transformers (vit) for blanket-penetrating sleep posture recognition using a triple ultra-wideband (uwb) radar system,” *Sensors*, vol. 23, no. 5, p. 2475, 2023.
- [34] Li *et al.*, “Advancing ir-uwb radar human activity recognition with swin-transformers and supervised contrastive learning,” *IEEE Internet of Things Journal*, 2023.
- [35] Kim *et al.*, “A study on 3d human pose estimation using through-wall ir-uwb radar and transformer,” *IEEE Access*, vol. 11, pp. 15 082–15 095, 2023.
- [36] Szegedy *et al.*, “Going deeper with convolutions,” in *Proceedings of the IEEE conference on computer vision and pattern recognition*, 2015, pp. 1–9.
- [37] He *et al.*, “Deep residual learning for image recognition,” in *Proceedings of the IEEE conference on computer vision and pattern recognition*, 2016, pp. 770–778.
- [38] Huang *et al.*, “Densely connected convolutional networks,” in *Proceedings of the IEEE conference on computer vision and pattern recognition*, 2017, pp. 4700–4708.
- [39] Howard *et al.*, “Mobilenets: Efficient convolutional neural networks for mobile vision applications,” *arXiv preprint arXiv:1704.04861*, 2017.
- [40] Touvron *et al.*, “Training data-efficient image transformers & distillation through attention,” in *International conference on machine learning*. PMLR, 2021, pp. 10 347–10 357.
- [41] Khan *et al.*, “Ir-uwb radar-based robust heart rate detection using a deep learning technique intended for vehicular applications,” *Electronics*, vol. 11, no. 16, p. 2505, 2022.
- [42] Morales-Alvarez *et al.*, “On transferability of driver observation models from simulated to real environments in autonomous cars,” in *2023 IEEE 26th International Conference on Intelligent Transportation Systems (ITSC)*. IEEE, 2023, pp. 3129–3134.
- [43] Stocco *et al.*, “Mind the gap! a study on the transferability of virtual versus physical-world testing of autonomous driving systems,” *IEEE Transactions on Software Engineering*, vol. 49, no. 4, pp. 1928–1940, 2022.
- [44] Gong *et al.*, “AST: Audio Spectrogram Transformer,” in *Proc. Interspeech 2021*, 2021, pp. 571–575.
- [45] Novelda, “Xethru X4M06 datasheet,” https://laonuri.techyneeti.com/wp-content/uploads/2019/02/X4M06_DATASHEET.pdf, [Online; accessed 17-June-2024].
- [46] GHSA, “Distracted driving,” <https://www.ghsa.org/state-laws-issues/distracted-driving>, [Online; accessed 12-April-2025].
- [47] CDC, “Distracted driving,” <https://www.cdc.gov/niosh/motor-vehicle/distracted-driving/index.html>, [Online; accessed 12-April-2025].
- [48] IIHS, “Distracted driving,” <https://www.iihs.org/topics/distracted-driving>, [Online; accessed 12-April-2025].
- [49] NIH, “Distracted driving,” <https://www.dolmanlaw.com/blog/smoking-driving-causes-distracted-driving-accidents-clearwater-fl>, [Online; accessed 12-April-2025].
- [50] W. using phone, “Distracted driving,” <https://www.who.int/publications/i/item/mobile-phone-use-a-growing-problem-of-driver-distraction>, [Online; accessed 12-April-2025].
- [51] Beck *et al.*, “xlstm: Extended long short-term memory,” *arXiv preprint arXiv:2405.04517*, 2024.
- [52] Deng *et al.*, “Imagenet: A large-scale hierarchical image database,” in *2009 IEEE conference on computer vision and pattern recognition*. Ieee, 2009, pp. 248–255.



Jeongjun Park received the B.S. degree from the Department of Information Communications Engineering, Hankuk University of Foreign Studies (HUFS), in 2018, and the M.S. and Ph.D. degree in Electrical and Computer Engineering from Seoul National University (SNU), Seoul, South Korea, in 2020 and 2025, respectively. He is currently with System LSI Business in Samsung Electronics. His research interests include the 5G/6G communication technologies, IoT, UWB, and AI.



Sunwook Hwang received the B.S. degree in Electrical Engineering from Pohang University of Science and Technology (POSTECH) in 2016 and the Ph.D. in Electrical and Computer Engineering from Seoul National University (SNU), Seoul, Korea, in August 2023. He served as a Post-Doctoral Researcher at SNU from September 2023 to August 2024. He is currently with Samsung Electronics, where his work focuses on Neural Processing Unit (NPU) design. His research interests include autonomous driving and computer vision.



Hyeonho Noh received the B.S. and the M.S. degrees in electrical engineering from Ulsan National Institute of Science and Technology (UNIST), Ulsan, South Korea, in 2018 and 2021, respectively, and received the Ph.D. degree in electrical engineering with the Pohang University of Science and Technology (POSTECH), Pohang, South Korea, in 2024. From Oct. 2024 to Jun. 2025, he worked as a post-doctoral researcher in the Department of Electrical Engineering, Seoul National University (SNU), Seoul, South Korea. He is currently an

Assistant Professor with the Department of Information and Communication Engineering, Hanbat National University, Daejeon, South Korea. His research interests include integrated sensing and communication and future wireless systems with deep neural networks.



Jin Mo Yang received the B.S. degree in electronic engineering from Hanyang University in 2018. He is currently pursuing the Ph.D. degree in electrical and computer engineering with Seoul National University. His research interests include video analytics, edge computing, and test-time adaptation (TTA) for evolving vision domains.



Hyun Jong Yang is an associate professor in the department of electrical and computer engineering, Seoul National University (SNU), Seoul, Korea. He received the B.S. degree in electrical engineering from Korea Advanced Institute of Science and Technology (KAIST), Korea, in 2004, and the M.S. and Ph.D. degrees in electrical engineering from KAIST, in 2006 and 2010, respectively. From Aug. 2010 to Aug. 2011, he was a research fellow at Korea Research Institute of Ships & Ocean Engineering (KRISO), Korea. From Oct. 2011 to Oct. 2012, he worked as a post-doctoral researcher in the Electrical Engineering Department, Stanford University, Stanford, CA. From Oct. 2012 to Aug. 2013, he was a Staff II Systems Design Engineer, Broadcom Corporation, Sunnyvale, CA, where he developed physical-layer algorithms for LTE-A MIMO receivers. In addition, he was a delegate of Broadcom in 3GPP RAN1 standard meetings. From Sept. 2013 to July 2020, he was an assistant/associate professor in the School of Electrical and Computer Engineering, UNIST, Korea. From July 2020 to Aug. 2024, he was an associate professor in the department of electrical engineering, Pohang University of Science and Technology (POSTECH), Pohang, Korea. Since Sept. 2024, he has been an associate professor in the department of electrical and computer engineering, Seoul National University (SNU), Seoul, Korea. His fields of interests are signal processing, wireless communications, and machine learning. Dr. Yang is an Editor for IEEE Wireless Communications Letters (WCL) and IEEE Internet of Things Journal (IoTJ), an Associate Editor-in-Chief for the Journal of Korean Institute of Communications and Information Sciences, and a Program Track Chair for the IEEE Consumer Communications & Networking Conference (CCNC) 2023 2025.



Saewoong Bahk (Senior Member, IEEE) received the B.S. and M.S. degrees in electrical engineering from Seoul National University (SNU), in 1984 and 1986, respectively, and the Ph.D. degree from the University of Pennsylvania, in 1991. He was with AT&T Bell Laboratories as a Member of Technical Staff, from 1991 to 1994, where he had worked on network management. From 2009 to 2011, he served as the Director of the Institute of New Media and Communications. He is currently a Professor at SNU. He has been leading many industrial projects

on 3G through 6G and IoT connectivity supported by the Korean industry. He has published more than 300 technical articles and holds more than 100 patents. He was a recipient of the KICS Haedong Scholar Award, in 2012. He was President of the Korean Institute of Communications and Information Sciences (KICS). He served as Chief Information Officer (CIO) of SNU. He was General Chair of the IEEE WCNC 2020 (Wireless Communication and Networking Conference), IEEE ICCE 2020 (International Conference on Communications and Electronics), and IEEE DySPAN 2018 (Dynamic Spectrum Access and Networks). He was TPC Chair of the IEEE VTC-Spring 2014, and General Chair of JCCI 2015. He was Director of the Asia-Pacific Region of the IEEE ComSoc. He is an Editor of the IEEE Network Magazine and IEEE Transactions on Vehicular Technology. He was Co-Editor-in-Chief of the Journal of Communications and Networks (JCN), and an editor of Computer Networks Journal and IEEE Tran. on Wireless Communications. He is a member of the National Academy of Engineering of Korea (NAEK).